Plexind1 negatively regulates zebrafish lymphatic development

Denver D. Britto[1], Jia He[2], June P. Misa[1], Wenxuan Chen[1], Purvi M. Kakadia[1, 3], Lin Grimm[4], Caitlin D. Herbert[1], Kathryn E. Crosier[1], Philip S. Crosier[1], Stefan K. Bohlander[1,3], Benjamin M. Hogan[4], Christopher J. Hall[1], Jesús Torres-Vázquez[2], Jonathan W. Astin[1,*]

[1]Department of Molecular Medicine & Pathology, School of Medical Sciences, University of Auckland, Auckland, New Zealand

[2]Skirball Institute of Biomolecular Medicine, New York University Grossman School of Medicine

[3]Leukaemia and Blood Cancer Research Unit, Department of Molecular Medicine & Pathology, Faculty of Medical and Health Sciences, The University of Auckland, Auckland, New Zealand

[4]Organogenesis and Cancer Program, Peter MacCallum Cancer Centre, Melbourne, Australia; Sir Peter MacCallum Department of Oncology, University of Melbourne, Australia; Department of Anatomy and Physiology, University of Melbourne, Australia

*Corresponding author: Jonathan Astin

Molecular Medicine & Pathology, The University of Auckland

Auckland 1142, New Zealand

Email: j.astin@auckland.ac.nz

Key words: Plexind1, Lymphatic, Zebrafish, Lymphangiogenesis, Vegfr

SUMMARY

Lymphangiogenesis is a dynamic process that involves the directed migration of lymphatic endothelial cells (LECs) to form lymphatic vessels. The molecular mechanisms that underpin lymphatic vessel patterning are not fully elucidated and, to date, no global regulator of lymphatic vessel guidance is known. In this study, we identify the transmembrane cell signalling receptor Plexind1 as a negative regulator of both lymphatic vessel guidance and lymphangiogenesis in zebrafish. *plxnd1* is expressed in developing lymphatics and is required for the guidance of both the trunk and facial lymphatic networks. Loss of *plxnd1* is associated with misguided intersegmental lymphatic vessel growth and aberrant facial lymphatic branches. Lymphatic guidance in the trunk is mediated, at least in part, by the Plxnd1 ligands, Semaphorin3aa and Semaphorin3c. Finally, we show that Plxnd1 normally antagonises Vegfr/Erk signalling to ensure the correct number of facial LECs and that loss of *plxnd1* results in facial lymphatic hyperplasia. As a global negative regulator of lymphatic vessel development, the Sema/Plxnd1 signalling pathway is a potential therapeutic target to treat diseases associated with dysregulated lymphatic growth.

INTRODUCTION

The lymphatic system is a network of vessels that are essential for interstitial fluid homeostasis with secondary roles in immune cell trafficking and lipid absorption. Dysregulated lymphangiogenesis has been implicated in a number of health conditions which include, lymphoedema (Brouillard et al., 2021; Saito et al., 2013), tumour metastasis (Stacker et al., 2014) and graft rejection (Dashkevich et al., 2016; Dietrich et al., 2010; Ishii et al., 2010; Pedersen et al., 2020; Wong, 2020).

Lymphatic endothelial cells (LECs), are mostly specified in the venous endothelium, via the action of the transcription factor PROX1 (Srinivasan et al., 2007; Wigle et al., 2002; Wigle and Oliver, 1999; Yaniv et al., 2006). The migration and proliferation of LECs is stimulated through VEGFR3 signalling in LECs, where the binding of VEGFC to VEGFR3 stimulates downstream signalling through the AKT/PI3K and MEK/ERK pathways to promote migration, proliferation and survival (Baek et al., 2019; Coso et al., 2012; Deng et al., 2015; Grimm et al., 2019; Hagerling et al., 2013; Hogan et al., 2009b; Karkkainen et al., 2004; Kuchler et al., 2006; Salameh et al., 2005; Shin et al., 2016). While the pathways that drive lymphangiogenesis are relatively well studied, the mechanisms that regulate this process are less well understood.

The ability to image the entire larval lymphatic network, *in vivo*, make zebrafish an ideal model to discover global regulators of lymphatic vessel growth (Jung et al., 2017; Okuda et al., 2012; Yaniv et al., 2006). In the zebrafish trunk, LECs migrate from the posterior cardinal vein (PCV) at 36 hpf to the horizontal myoseptum to form parachordal LECs (Bussmann et al., 2010; Hogan et al., 2009a; Yaniv et al., 2006). These parachordal LECs then migrate along the arterial intersegmental blood vessels (aISVs) to form the trunk lymphatic network, which by 6 dpf consists of intersegmental lymphatic vessels (ISLVs), the thoracic duct (TD) and the dorsal longitudinal lymphatic vessel (Bussmann et al., 2010; Okuda et al., 2012). In the zebrafish head, facial LECs are specified in the common cardinal vein, primary head sinus and from a non-venous progenitor called the ventral aortal lymphangioblast. By 6 dpf these progenitors have coalesced to form the otolithic lymphatic vessel (OLV), the medial facial lymphatic (MFL), and lateral facial lymphatic (LFL) (Eng et al.,

2019; Okuda et al., 2012). Importantly, all of these vessels form in a reproducible pattern with little individual variation, suggesting that the migration and growth of both the trunk and facial lymphatic guidance is tightly regulated. It is known that specific populations of neurons, arterial mural cells and fibroblasts are required for growth of lymphatics in the zebrafish trunk and that both mature Vegfc and the chemokine ligands Cxcl12a/ Cxcl12b are involved in mediating the aISV/LEC interaction in the zebrafish trunk (Cha et al., 2012; Lim et al., 2011; Peng et al., 2022; Wang et al., 2020). However, to date no global regulator of lymphatic vessel guidance has been identified.

We conducted a forward genetic screen to identify novel regulators of lymphatic development and uncovered a loss-of-function *plexind1* mutant displaying a novel lymphatic misguidance and overgrowth phenotype. PLXND1 is part of a family of large transmembrane cell-signalling receptors that have roles in both axon and vascular guidance (Zhang et al., 2021). PLXND1 is expressed within endothelial cells and is activated primarily by binding to either secreted or membrane-tethered Semaphorin (SEMA) ligands, which results in modulation of endothelial cell migration, growth and adhesion. Previous work has shown that PLXND1 has a conserved role in inhibiting the growth of blood vessels through antagonising VEGFR signalling and by regulating actin polymerisation within endothelial cells (Childs et al., 2002; Fukushima et al., 2011; Gitler et al., 2004; Gu et al., 2005; Kim et al., 2011; Moriya et al., 2010; Tata et al., 2014; Torres-Vazquez et al., 2004; Zhang et al., 2009; Zygmunt et al., 2011). While the molecular mechanisms that underpin PLXND1-mediated anti-angiogenesis are still not clear, it is thought that upon ligand binding, the GTPase activating protein (GAP) domain of PLXND1 is activated leading to the deactivation of Rho-GTPases, resulting in the disruption of integrin-mediated cell

adhesion, downregulation of both ERK and MAPK signalling and modulation of the actin cytoskeleton (Gay et al., 2011; Zhang et al., 2021). In mice, SEMA3C, SEMA3D and SEMA4A have all been implicated in the negative regulation of blood vessel growth through PLXND1 (Gu et al., 2005; Toyofuku et al., 2007; Yang et al., 2015). In zebrafish, Sema3/Plxnd1 signalling is essential for intersegmental blood vessel (ISV) guidance; Sema3aa and Sema3ab are expressed within the somites and this restricts ISV development to the intersomitic boundaries (Childs et al., 2002; Torres-Vazquez et al., 2004). In addition, the development of the zebrafish common cardinal vein, which requires collective endothelial cell migration, is guided by repulsive cues provided by Sema3d/Plxnd1signalling (Hamm et al., 2016). Knockdown of mouse *Plxnd1* demonstrated that it also has a role in lymphatic development. SEMA3G expressed by dermal arteries provides a repulsive cue to PLXND1-expressing LECs and knockout of either PLXND1 or SEMA3G resulted in the dermal lymphatics being aligned more closely with dermal blood vessels (Liu et al., 2016), while PLXND1 mutants have additional lymphatic precursors in the intersomitic vessels and display extra branching in the developing cardiac lymphatics (Maruyama et al., 2021; Yang et al., 2012).

In this study we show that loss of zebrafish Plxnd1 function results in misguided ISLVs, aberrant branching of the facial lymphatics and an increase in the number of facial LECs. Together our data shows that Plxnd1 transduces repulsive Sema3 signals to guide lymphatic vessels and limit lymphangiogenesis and is therefore a potential pathway that can be manipulated to control lymphatic vessel growth.

RESULTS

plexind1 mutants have uncontrolled lymphatic vessel growth

We conducted a forward genetic screen in the lymphatic-marking *lyve1b:DsRed* transgenic zebrafish line (Okuda et al., 2012)with the aim of identifying genes that regulate lymphatic vessel development. From this screen, we identified a recessive mutant (*nz75*) that displayed non-stereotypical growth of the lymphatics in the trunk and the head (Fig. 1) – a phenotype that had not been previously described in zebrafish lymphatic mutants. Mutants were viable and fertile as adults and displayed no gross abnormalities (Fig. S1).

Using whole genome sequencing coupled with SNP homozygosity linkage analysis (Leshchiner et al., 2012), we mapped the causative mutation to a 600 kb region at the telomeric region of chromosome 8. Within this region was the gene *plexind1* (*plxnd1*) which had been previously implicated in blood vessel guidance and was therefore a clear candidate (Fig. S1). Sequencing the coding regions of *plxnd1* in the mutant revealed a single nucleotide substitution of thymine to guanine in the mutant, resulting in an amino acid change from isoleucine to serine in residue 1030 within the third IPT domain of Plxnd1 (Fig. S1). This residue is highly conserved and secondary structure prediction revealed that this mutation is likely to destabilize ß-sheet formation leading to a reduction-of-function (Fig. S1).

Plxnd1 has previously been shown to regulate blood vessel development, with the *out of bounds* (*plxnd1*^{fov01b}) mutant displaying aberrant intersegmental blood vessel (ISV) growth (Childs et al., 2002; Torres-Vazquez et al., 2004). Consistent with this, our *plxnd1*^{nz75} mutants displayed a phenotype of abnormally patterned intersegmental blood vessels (ISVs). In wild type animals, the primary ISVs emerged from the DA at the intersomitic boundaries and had no additional branches emerging from the main

ISV (Fig. S2). In contrast, *plxnd1*^{nz75} mutant fish displayed aberrant ISVs emerging at various locations across the DA and each ISV had subbranches (Fig. S2). This phenotype was also observed in wild type fish subjected to morpholino-mediated *plxnd1*-knockdown. The blood vessel phenotype was quantitated using two measures. Aberrant ISVs were defined as any ISV arising from the DA in a mid-somitic position. The second involved counting the number of branchpoints for each ISV at 36 hpf. *plxnd1*^{nz75} mutant fish both displayed an 10-fold increase in the number of aberrant ISVs and 11-fold increase in ISV branchpoints (Fig. S2). While a similar phenotype was observed in both *plxnd1* morphants and *plxnd1*^{fov01b} mutants, the severity of the ISV branching phenotype was significantly higher in both the *plxnd1*^{fov01b} mutant and *plxnd1* morphants (18-fold increase in morphants, 16-fold in *fov01b* mutants vs 11-fold in *nz75* mutants) suggesting that the *plxnd1*^{nz75} allele is a partial loss-of-function (Fig. S2). Importantly, *plxnd1* mutant and morphant embryos displaying this blood vessel phenotype completely segregated with the previously observed lymphatic phenotype (Fig. 1) suggesting that *plxnd1* is responsible for both blood and lymphatic vessel patterning.

Plxnd1 regulates secondary angiogenic sprouting

We and others have demonstrated that there is an increase in primary angiogenesis (sprouting from the DA) in *plxnd1*^{nz75} mutants and morphants (Fig. S2) (Torres-Vazquez et al., 2004), but the role of Plxnd1 signalling in secondary angiogenesis (sprouting from the PCV) was unknown. In order to investigate this, we imaged *lyve1b:EGFP* larvae at 39 hpf – a timepoint when secondary sprouts are emerging from the PCV and observed an approximate 1.5-fold increase in secondary angiogenic sprouts in both *plxnd1*^{nz75} mutants and morphants (Fig. S3). Normally, half of these

secondary sprouts contribute to the trunk lymphatic network by migrating to form parachordal LECs (PLs) at the horizontal myoseptum, while the other half anastomose with nearby ISVs to create veins (Geudens et al., 2019; Hogan et al., 2009b). We therefore examined both PL formation at 48 hpf as well as the number and ratio of arterial and venous ISVs in both *plxnd1*^{nz75} mutants and morphants. Surprisingly, we found no increase in PL number in either *plxnd1*^{nz75}mutants or morphants (Fig. S3). Instead, we found that there was an approximate 2-fold increase in the number of venous ISVs which, because of the corresponding earlier increase in primary sprouting (Fig. S2) resulting in a 2-fold increase in arterial ISVs, maintains a 1:1 arterial:venous ISV ratio in 72 hpf *plxnd1* animals (Fig. S3). This data indicates that the additional secondary sprouting in *plxnd1* mutants contributes towards the trunk blood vascular network.

Plxnd1 acts as a lymphatic guidance factor

We noted that there were mispatterned intersegmental lymphatic vessels (ISLVs) in *plxnd1*^{nz75} mutants and morphants at 6 dpf (Fig. 1A-F). The ISLVs are typically guided during their development by growing along arterial ISVs (aISVs) and therefore the pattern of ISLV growth is normally congruent with the underlying pattern of aISVs (Bussmann et al., 2010). There are two explanations for the mispatterned ISLVs we observed in *plxnd1*^{nz75} animals. The first explanation is that the ISLVs are mispatterned indirectly, due to the ISV defect induced by loss of *plxnd1* (Fig. S2), in which case the lymphatics will still align with the ISVs. The second explanation is that *plxnd1* is directly required for ISLV guidance in which case the lymphatics will develop independently from the ISVs. To distinguish between these two possibilities, we quantitated the percentage of ISLVs that did not align with an

ISV in double transgenic *lyve1b:DsRed; kdrl:EGFP* larvae. While wild type and control morpholino-treated larvae almost never displayed ISLVs that were misaligned with ISVs (96% and 94% ISLV-ISV alignment respectively), ISLVs were frequently observed in both *plxnd1*^{nz75} mutants and morphants developing distinct from the ISVs (52% and 58% ISLV-ISV alignment respectively), suggesting that *plxnd1* is directly required for correct ISLV patterning (Fig. 1E). *plxnd1*$^{nz75/fov01b}$ trans-heterozygotes also displayed an increase in misaligned ISLVs (59% ISLV-ISV alignment) Fig. 1E), confirming that the ISLV misguidance phenotype was caused by loss of *plxnd1*.

We further examined the facial lymphatic phenotype at 6 dpf in *plxnd1*^{nz75} mutants and in *plxnd1* morphants. Any facial lymphatic branches that are not usually observed in wild type animals were considered aberrant. We noted that *plxnd1* animals frequently displayed aberrant branches from vessels within the facial lymphatic network (Fig. 1C-D). Quantitation revealed that *plxnd1*^{nz75} mutants had 5-fold increase in the number of aberrant facial lymphatic branches (Fig. 1F) suggesting that *plxnd1* normally prevents excessive facial lymphatic growth. *plxnd1*$^{nz75/fov01b}$ trans-heterozygotes also displayed a 3-fold increase in aberrant facial lymphatic branches (Fig. 1F), confirming that this phenotype was caused by the loss of *plxnd1*.

To further confirm the ISLV misguidance phenotype, we examined ISLV patterning in *soluble flt1* (*sflt1*) morphants. sFlt1 normally inhibits blood vessel growth by binding and sequestering Vegfa ligands and therefore knockdown of this gene is known to cause aberrant growth of ISVs, but sFlt1 is not able to bind either Vegfd or Vegfc and is not predicted to directly influence ISLV growth (Krueger et al., 2011; Vogrin et al., 2019). A previously validated *sflt1* splice-blocking morpholino

(Krueger et al., 2011; Wild et al., 2017) was injected into *lyve1b:DsRed; kdrl:EGFP* fish and the blood and lymphatic vessels in the trunks of these larvae were imaged at 6 dpf. Despite the expected 11-fold increase in ISV branching, there was no accompanying increase in misaligned ISLVs in *sflt1* morphants (Fig. S4). This demonstrates that ectopic ISV growth is not sufficient to uncouple ISLV guidance from the ISVs and provides further evidence for the direct guidance of ISLV growth by Plxnd1.

We examined the ISLV misguidance phenotype in detail by performing time-lapse imaging of both wild type (Movie 1) and *plxnd1*^{nz75} (Movie 2) animals from 60 to 70 hpf – when the parachordal LECs normally migrate from the horizontal myoseptum (HM) to form ISLVs alongside adjacent aISVs (Bussmann et al., 2010). In wild type larvae, the developing ISLVs began migrating from the HM at the junction with each aISV but in *plxnd1*^{nz75} larvae, the developing ISLVs would frequently migrate out of the HM at other locations (Fig. 2A-J). Furthermore, while wild type ISLVs spent almost 100% of their migration path aligned with aISVs, in *plxnd1*^{nz75} larvae they only spent 60% of their time in contact with an artery (Fig. 2K). Consequently, the developing ISLVs in *plxnd1*^{nz75} larvae often deviate from the ventral-to-dorsal growth trajectory characteristic of wild types, instead growing in an anterior or posterior direction, as shown by the traces displaying the ISLV growth paths. (Fig. 2I-J). Finally, while in wild type larvae the developing ISLV generally had a single growing tip and therefore one direction of migration, in *plxnd1*^{nz75} larvae the developing ISLVs were frequently observed to have multiple tips, with a four-fold increase in branching events per hour (Fig. 2L). The vessel tips would also frequently regress and change direction, taking a tortuous path to reach their final position, as seen by the

1.8-fold increase in ISLV meandering behaviour in *plxnd1*^{nz75} larvae (Fig. 2M). Taken together this data shows that Plxnd1 normally functions to restrict lymphatic vessel migration to ensure the stereotypical pattern of the trunk and head lymphatic networks.

Plxnd1 acts cell autonomously to regulate lymphatic vessel guidance

Our data indicates that Plxnd1 signalling regulates lymphatic vessel guidance. To test if Plxnd1 performs this role in a cell autonomous fashion, we first confirmed that *plxnd1* is expressed in developing zebrafish lymphatic vessels by performing whole mount *in situ* hybridisation. We observed *plxnd1* expression in the trunk blood vasculature at 36 hpf as shown previously (Fig. S5) (Torres-Vazquez et al., 2004). In *lyve1b:EGFP* embryos at 48 hpf - a timepoint when the developing facial and trunk lymphatics can be visualised using an anti-*EGFP* probe (Okuda et al., 2012) we observed *plxnd1* expression in both the facial lymphatic sprout in the head and in the parachordal LECs in the trunk, confirming that *plxnd1* is expressed in zebrafish LECs during lymphatic vessel development (Fig. 3A-B, Movies 3 and 4).

Next we investigated whether Plxnd1 acts cell autonomously within LECs. In order to test this hypothesis, transplantations were performed between *plxnd1*^{nz75} donors and wild type hosts at the blastula stage. If *plxnd1* acts cell autonomously to guide lymphatic growth then *plxnd1*^{nz75} donor LECs would be expected to grow ectopically in wild type hosts. To visualise the origin and fate of donor-derived endothelium, cells were transplanted from *lyve1b:DsRed; kdrl:EGFP* donor embryos into *fli1a:EGFP* host embryos (Fig. 3C). The expression of DsRed in the host embryos allowed the visualisation of donor-derived LECs at 6 dpf, while EGFP expression

allowed visualisation of both host (*fli1a:EGFP*) and donor-derived (*kdrl:EGFP*) blood ECs at 6 dpf. In this way, it could be determined whether donor LECs are being guided normally by growing along blood vessels or if they are misaligned with either host or donor derived blood ECs. The transplants were conducted using donor and host blastula embryos at 3 hpf. Chimeric embryos were raised and the facial and trunk vasculature imaged at 6 dpf.

As expected, wild type LECs in wild type hosts did not form aberrant branches in the facial lymphatics and did not result in misaligned ISLVs (Fig. 3D, F, H, I). In contrast, *plxnd1*^{nz75} LECs in wild type hosts displayed an 1.8-fold increase in the number of aberrant branches from *plxnd1*^{nz75} (*lyve1b:DsRed*-expressing) facial vessels. In the trunk, only 66% of *plxnd1*^{nz75} (*lyve1b:DsRed*-expressing) ISLVs were correctly aligned with aISVs, compared to 99% of wild type (*fli1a:EGFP*-expressing) host ISLVs (Fig. 3E, G, H, I). Finally, there was a 9-fold increase in aberrant ISV growth in the *plxnd1*^{nz75} mosaic animals, which was consistent with role of *plxnd1* in regulating ISV migration (Childs et al., 2002; Torres-Vazquez et al., 2004), (Fig. S5). Overall our results indicate that *plxnd1* is acting cell autonomously within LECs to guide lymphatic vessel growth.

Plxnd1 antagonises Vegfr-signalling to regulate facial lymphatic growth

We also noted an additional phenotype in the facial lymphatics of our *plxnd1*^{nz75} mutant and morphants. At 6 dpf the facial lymphatics appeared thickened, with enlarged LFLs, MFLs and OLVs when compared with controls – suggesting an increase in the number of facial LECs. To test this, we generated double transgenic *lyve1b:DsRed; fli1a:nlsEGFP* fish and counted the number of facial LECs (fLECS)

present at 6 dpf. This revealed that the *plxnd1*^{nz75} mutants and morphants had approximately 16% more fLECs than controls (Fig. 4A-C). This phenotype was also observed in *plxnd1*$^{nz75/fov01b}$ trans-heterozygotes (24% increase in fLECs over wild type), confirming that the loss of Plxnd1 signalling results in facial lymphatic hyperplasia. To define when facial lymphatic hyperplasia occurs in the mutants, wild type and *plxnd1*^{nz75} larvae were imaged at 3, 4, 5 and 6 dpf, with the *plxnd1*^{nz75} larvae displaying significantly more facial LECs at 4 and 6 dpf (Fig. 4D). Next, we examined the numbers of *prox1a*-expressing lymphatic progenitors in the head and observed no difference between *plxnd1*^{nz75} mutants and wild type (Fig. S6). Taken together this data shows that the facial lymphatic hyperplasia in *plxnd1*^{nz75} animals occurs after lymphatic specification and sprouting. We also quantitated trunk LECs at 6 dpf, as well as *prox1a*-expressing lymphatic progenitor formation in the PCV at 36 hpf, and found no evidence of either trunk lymphatic hyperplasia or an increase in lymphatic progenitors (Fig. 4E, Fig. S6) – a result consistent with our earlier analysis showing normal numbers of parachordal LECs in *plxnd1*^{nz75} animals (Fig. S3).

We next determined if the facial lymphatic hyperplasia phenotype depends on Vegfr signalling. To test this, we used two small molecule inhibitors - sunitinib (a tyrosine kinase inhibitor) and tivozanib (a specific VEGFR inhibitor), that block lymphatic vessel growth in zebrafish (Okuda et al., 2015). *lyve1b:DsRed; fli1a:nlsEGFP* larvae were placed into a solution of either DMSO, 1 µM sunitinib or 2 nM tivozanib at 3 dpf – a timepoint prior to the onset of the hyperplasia phenotype and maintained in these compounds until 6 dpf when they were analysed. These inhibitor concentrations were chosen as they are the highest doses that still allowed the complete development of both the facial and trunk lymphatic networks. Drug-treated wild type larvae

displayed a modest reduction in the average number of fLECs (DMSO = 78, sunitinib 60, tivozanib = 64) – a result consistent with inhibition of Vegfr signalling, while inhibitor treatment of *plxnd1*^{nz75} larvae was able to rescue the facial lymphatic hyperplasia by normalising facial LEC numbers (*plxnd1*+ DMSO = 88, *plxnd1*+ sunitinib = 63, *plxnd1*+ tivozanib = 70). This rescue suggests that elevated Vegfr signalling drives the facial lymphatic hyperplasia phenotype seen in *plxnd1*^{nz75} larvae (Fig. 5A). Of note, when the same level of Vegfr inhibition was applied from 2 -6 dpf it had no significant effect on either the number of aberrant facial lymphatic branches or in the degree of misalignment of the ISLVs at 6 dpf, suggesting that dysregulated Vegfr signalling is not responsible for the misguidance of lymphatics in *plxnd1*^{nz75} mutants (Fig. S7).

In order to investigate which signalling pathway downstream of Vegfr is overactivated in *plxnd1* larvae, we examined the activity of the MEK/ERK pathway, as it is known to be inhibited by SEMA3/PLXND1, is downstream of VEGFR function, and is also known to promote cell proliferation and survival in LECs (Baek et al., 2019; Carretero-Ortega et al., 2019; Grimm et al., 2019; Shin et al., 2016; Wortzel and Seger, 2011). Erk activity was measured by immunostaining against phospho-Erk (pErk) and anti-EGFP in 36 hpf *lyve1b:EGFP* larvae. The percentage of pErk-positive cells in the PCV of *plxnd1* morphants was increased to 61% compared to only 39% in control morphants, indicating that the higher levels of secondary sprouting seen upon the loss of Plxnd1 may be a result of increased Erk signalling within the PCV (Fig. 5B). We then investigated Erk activity in the facial lymphatics at 3 dpf (Fig. 5C-E) and observed a significant increase in the proportion of pErk-positive fLECs in *plxnd1* morphants (36% of fLECs were pErk-positive) over control

morphants (20% of fLECs were pErk-positive) (Fig. 5C-E). To test the role of the Mek/Erk pathway in facial lymphatic hyperplasia phenotype, wild type and *plxnd1*^{nz75} larvae were treated with 5 µM of the MEK inhibitor SL327 from 3 to 6 dpf. This dose was chosen as it is the highest possible dose that still allowed the complete development of the facial lymphatic network. Inhibition of Mek signalling was able to rescue the facial lymphatic hyperplasia phenotype in *plxnd1*^{nz75} larvae, with fLEC number reduced to wild type levels (WT + DMSO = 75, *plxnd1*^{nz75} = 86, *plxnd1*^{nz75} + SL327 = 71) (Fig. 5F), indicating that Plxnd1 signalling normally antagonises Vegfr signalling though the Mek/Erk pathway in order to limit fLEC numbers.

It was intriguing that lymphatic hyperplasia was only observed in the facial lymphatic network. One of the key differences between facial and trunk lymphatic development is that the facial lymphatics require Vegfd-induced Kdr signalling (Astin et al., 2014a; Bower et al., 2017; Vogrin et al., 2019). We hypothesised that Plxnd1 might normally antagonise Kdr-driven Erk signalling, which results in a specific facial lymphatic hyperplasia phenotype when *plxnd1* is lost. As Vegfd has been shown to only bind to Kdr (Vogrin et al., 2019), we predicted that *plxnd1* mutants should be resistant to *vegfd* knockdown. To test this, *lyve1b:DsRed; fli1a:nlsEGFP* wild type or *plxnd1*^{nz75} embryos were injected with either control morpholino or a previously validated *vegfd* morpholino (Astin et al., 2014a; Bower et al., 2017) and the fLECs were quantified. We found that, as expected, *vegfd* knockdown resulted in a 15% reduction in fLECs in wild type larvae but, by contrast, there was no significant reduction in fLEC numbers in *plxnd1*^{nz75} mutants (Fig. 5G). Taken together these data suggest that Plxnd1 signalling normally antagonises Kdr-driven Mek/Erk signalling to limit fLEC numbers.

Sema3 ligands regulate trunk lymphatic development

Plxnd1 is thought to negatively regulate ISV growth through the ligands Sema3aa and Sema3ab (Torres-Vazquez et al., 2004). These secreted Sema ligands are expressed from the somites where they could bind to and activate Plxnd1 signalling in the blood endothelial cells to prevent aberrent growth of the ISVs into the adjacent somites (Torres-Vazquez et al., 2004). Given the similarity in phenotype between the blood and lymphatic misguidance phenotypes in the trunk we wondered if these ligands may also be required for ISLV guidance. We first confirmed that both *sema3aa* and *sema3ab* are expressed in the somites by whole mount *in situ* hybridisation at 24 hpf. While we were unable to observe a reliable *in situ* signal for either gene at 30 or 48 hpf, RT-PCR confirmed that both of these genes are expressed in both the head and trunk at 48 hpf during lymphatic development (Fig S8).

We analysed a *sema3aa*^{sa10241} mutant generated by The Zebrafish Mutation Project (Kettleborough et al., 2013). This mutant contains a C to T substitution that converts Gln501 into a premature stop codon, truncating the protein by 359 aa within the Semaphorin domain. We observed a significant increase in the frequency of misaligned ISLVs in *sema3aa*^{sa10241} mutant embryos when compared to WT (WT = 95% ISLV-ISV alignment, *sema3aa* = 78% ISLV-ISV alignment) (Fig. 6A-G), demonstrating that Sema3aa ligands are involved in the Plxnd1-mediated guidance of ISLV growth. However, *sema3aa*^{sa10241} mutants had no increase in aberrant facial lymphatic branches or in the number of fLECs (Fig. 6B, H-I) suggesting that the role of this ligand is restricted to the trunk lymphatic development.

Sema3c has been previously shown to be expressed in the head during facial lymphatic development (Callander et al., 2007; Yu and Moens, 2005) and was therefore a candidate Plxnd1 ligand to be involved in facial lymphatic growth and guidance. Whole mount *in situ* hybridisation at 24 and 30 hpf showed that *sema3c* was also expressed in neuronal cells in the trunk and RT-PCR from both head and trunk RNA confirmed that expression was maintained in both the head and trunk at 48 hpf during lymphatic vessel development (Fig S8). A *sema3c*^{sa15161} mutant generated by The Zebrafish Mutation Project (Kettleborough et al., 2013) was obtained. This mutant contains a C to A substitution that converts Ser142 and Ser186 in the 713 and 757aa Sema3c isoforms into a premature stop codon, thus truncating these proteins within the Semaphorin domain. We observed a significant increase in misaligned ISLVs in the trunk of *sema3c*^{sa15161} mutants (WT = 95% ISLV-ISV alignment, *sema3c* = 70% ISLV-ISV alignment) (Fig. 6D-G), demonstrating that multiple Sema3 ligands are involved in the guidance of ISLV growth. However, Sema3c mutants had no facial lymphatic defects (Fig. 6C, H-I) suggesting that *sema3c* is not required for facial lymphatic development.

DISCUSSION

We have shown that Plxnd1 acts cell autonomously in LECs to guide the pathfinding of the facial and trunk lymphatic networks (Fig. 7). In addition, we uncovered a role for *plxnd1* as a negative regulator of facial lymphangiogenesis. We show that loss of *plxnd1* results in facial lymphatic hyperplasia and that Plxnd1 normally antagonises Vegfr/Erk signalling to ensure the correct number of facial LECs (Fig. 7).

In the zebrafish trunk, the ISLVs are normally aligned with the aISVs (Bussmann et al., 2010). This interaction is, in part, mediated by chemokine signalling; Cxcl12b

ligands, which are secreted from aISVs and associated mural cells, activate signalling in the Cxcr4a/b-expressing LECs that helps to anchor their migration along the aISV (Cha et al., 2012; Peng et al., 2022). We showed that the loss of Plxnd1 function results in growth of ISLVs away from the blood vessels and across the somites. Live imaging revealed that growing ISLVs in *plxnd1* larvae were more dynamic, spent significantly less time aligned with aISVs and in some instances even migrated directly across them. This suggests that the negative guidance provided by Plxnd1 signalling is the dominant guidance cue for the correct patterning of ISLVs.

We have also identified two Sema ligands involved in ISLV guidance; *sema3aa* mutants and *sema3c* mutants both displayed misguided ISLVs similar to those observed in *plxnd1* mutants. We have confirmed that *sema3aa* is expressed in somites prior to lymphatic development (Torres-Vazquez et al., 2004) and that its expression is maintained in the trunk from 22 - 48 hpf. We have also shown that *sema3c* is expressed within the trunk at 48 hpf and observed expression in trunk neuronal structures by *in situ* hybridisation at 24 - 30 hpf. It is therefore likely that the expression of Sema ligands within the somitic region activates repulsive Plxnd1 signalling in LECs that grow towards the somite, restricting their growth to align with the aISVs within the intersomitic space (Fig. 7). The ISLV misguidance phenotype was less severe in both *sema3* mutants than in *plxnd1*-deficient larvae, suggesting that they act redundantly, likely with other Sema ligands (such as Sema3ab), to regulate ISLV guidance. The role of Sema3/Plxnd1 signalling in the zebrafish trunk lymphatics is similar to its role in patterning the murine lymphatics. SEMA3G ligands released by arteries has been shown to repel PLXND1-expressing dermal lymphatics (Liu et al., 2016). In addition, loss of PLXND1 causes an increase in the branching of

the cardiac lymphatic plexus around the truncus arteriosus (Maruyama et al., 2021). Taken together with our data, this demonstrates that PLXND1/SEMA signalling has a conserved role in lymphatic guidance.

The facial lymphatics, which are not guided by blood vessels, were also mispatterned in *plxnd1* larvae, with an increase in aberrant branches that was similar to the phenotype observed in the trunk. Neither *sema3aa* or *sema3c* appear to involved in facial lymphatic guidance despite both of these ligands being expressed in the head (Fig S8), (Callander et al., 2007; Tanaka et al., 2007). The role and identity of Sema ligands involved in facial lymphatic guidance remains to be determined.

PLXND1 has a conserved role as a negative regulator of angiogenesis. It regulates blood vessel growth by antagonising VEGFR signalling and also by directly regulating cell migration through destabilising actin polymerisation and integrin-mediated cell adhesion in endothelial cells (Childs et al., 2002; Fukushima et al., 2011; Gitler et al., 2004; Gu et al., 2005; Kim et al., 2011; Maruyama et al., 2021; Moriya et al., 2010; Tata et al., 2014; Torres-Vazquez et al., 2004; Zhang et al., 2009; Zygmunt et al., 2011). We show that suppression of Vegfr signalling did not normalise the lymphatic misguidance phenotype in the trunk or the head. This data suggests that Plxnd1 inhibits pro-migration pathways that are somewhat independent of Vegfr signalling, such as actin assembly and the formation of integrin-mediated adhesions (Driessens et al., 2001; Tata et al., 2014). There are a number of intracellular modulators associated with PLXND1 signalling such as Rho-GTPases, endocytic adaptors of the GIPC family, cytoskeletal proteins, integrins and kinases that have been associated with PLXND1 regulation of cell growth that could be

involved in lymphatic guidance (Burk et al., 2017; Carretero-Ortega et al., 2019; Choi et al., 2014; Sakurai et al., 2010; Sakurai et al., 2011; Tata et al., 2014; Uesugi et al., 2009; Wang et al., 2012). *In vitro* studies have shown that SEMA3E-PLXND1 signalling inhibits the formation of actin stress fibres and focal adhesions which results in reduced motility and retraction of LECs (Liu et al., 2016; Maruyama et al., 2021). It is therefore possible that activation of Plxnd1 signalling causes localised disruption of the cell migration machinery leading to withdrawal of cell protrusions and directed growth of the developing lymphatic vessel away from areas containing Sema3 ligands. Future experiments will focus on uncovering the downstream lymphatic migration pathways regulated by Plxnd1.

Plxnd1 signalling can also act as a negative regulator of lymphangiogenesis, which, unlike its guidance role, is context-specific; loss of *plxnd1* caused an increase in the number of facial LECs but had no effect on trunk LECs. Unlike the misguidance phenotype, the facial lymphatic hyperplasia was normalised by suppression of either Vegfr or Mapk/Erk signalling, indicating that Plxnd1 signalling normally antagonises this pathway. In support of this, we observed an increase in Erk signalling within the fLECs of *plxnd1* morphant larvae. Plexins regulate MAP/ERK signalling in a various contexts (Aurandt et al., 2006; Basile et al., 2007; Bribian et al., 2014; Ito et al., 2014). In addition, SEMA3E/PLXND1 signalling is known to inhibit VEGFR-mediated and VEGFR-independent ERK signalling in blood endothelial cells (Carretero-Ortega et al., 2019; Moriya et al., 2010) and has been shown to inhibit LEC cell proliferation (Maruyama et al., 2021; Yang et al., 2012). However the exact molecular mechanism by which PLXND1 antagonises VEGFR signalling is not yet established.

One of the key differences between trunk and facial lymphatic development is the specific requirement for Vegfd/Kdr signalling in the development of the facial lymphatics (Astin et al., 2014a; Bower et al., 2017; Vogrin et al., 2019). We therefore hypothesised that Plxnd1 limits Kdr-signalling and thus inactivation of *plxnd1* leads to facial lymphatic hyperplasia. In support of this, *plxnd1*^{nz75} animals were resistant to morpholino knockdown of *vegfd*, a Kdr-specific ligand. Together our data suggest that Plxnd1 antagonises Kdr/Vegfr signalling to limit lymphatic growth.

While Plxnd1 is known to regulate primary angiogenic sprouting (Childs et al., 2002; Torres-Vazquez et al., 2004), we show that it also regulates secondary sprouting from the posterior cardinal vein. Interestingly, despite an increase in secondary sprouting there was no change in the number of Prox1-expressing lymphatic progenitors within the PCV or in parachordal LEC formation in our *plxnd1*^{nz75} mutant fish. Instead, the extra secondary sprouts were biased towards a venous fate to match the earlier increase in primary sprouting from the DA. This resulted in a roughly 2-fold increase in the number of both aISVs and vISVs and therefore the ratio of aISVs to vISVs was unchanged in *plxnd1*^{nz75} mutants. This observation supports previous studies which show that the balance between arterial and venous ISVs is tightly regulated (Bussmann et al., 2010; Geudens et al., 2019; Geudens et al., 2010).

It has been shown that the arteriovenous fate of ISVs is determined by the levels of Notch signalling in the primary ISVs and by an adaptive flow-mediated mechanism that together ensure a 1:1 ratio of arteries to veins (Geudens et al., 2019). Therefore, the fate of each secondary sprout is largely determined by the fate of the ISV that it

engages with. While Prox1a signalling is required for lymphatic specification (Koltowska et al., 2015; Nicenboim et al., 2015), live imaging has revealed that lymphatic progenitors can arise from secondary sprouts that form no stable connection with an ISV (non-venous) but also from secondary sprouts that connect to an ISV and become venous (Geudens et al., 2019; Isogai et al., 2003). Together these data support the idea that the mechanisms that promote the formation of secondary sprouts are distinct from the mechanisms involved in determining their fate. Our data suggests that while *plxnd1* normally inhibits secondary sprouting, likely by antagonising the Vegfr3/Erk pathway, *plxnd1* does not regulate arterial-venous fate decisions or the induction of Prox1a and lymphatic fate.

We have shown that Plxnd1 is an important regulator of developing lymphatics in zebrafish. The severity of the misguidance phenotype in *plxnd1* mutants suggests that Sema3/Plxnd1 signalling plays a major role in shaping the anatomy of the lymphatic network. We have also identified a role for *plxnd1* as an inhibitor of lymphangiogenesis by antagonising Kdr/Vegfr signalling within fLECs. This data demonstrates that not only is lymphatic migration regulated by *plxnd1* but that, in certain contexts, it is also required to ensure the correct levels of lymphangiogenesis. Based on previously observed conservation of PLXND1 function it is highly likely that it also acts as broad regulator of lymphatic growth in mammals (Liu et al., 2016; Maruyama et al., 2021; Yang et al., 2012). Dysregulated lymphatic development underpins a number of human health conditions; lymphatic overgrowth in tumours is associated with metastasis, while lack of lymphatic regeneration following lymph node removal promotes cancer-associated secondary lymphoedema (Gousopoulos et al., 2017; Saito et al., 2013; Yoon et al., 2003). Currently, the VEGFC/VEGFR3

pathway is the key target for regulating lymphatic development. Our data identifies the PLXND1 pathway as a potential additional therapeutic target in the treatment of lymphatic pathologies. The use of antibodies, shRNA, injection of ligands, or cell-permeable peptides that target PLXND1's cytosolic domain could be used to inhibit or stimulate PLXND1 signalling in order to therapeutically promote or suppress lymphangiogenesis (Dieterich and Detmar, 2015; Fukushima et al., 2011; Moriya et al., 2010; Stacker et al., 2014; Vivekanandhan et al., 2021; Zhou et al., 2018). Importantly, therapeutically targeting PLXND1 can likely synergise with existing strategies targeting the VEGFC/VEGFR3 pathway and allow additional therapeutic control of lymphatic growth.

METHODS

Zebrafish lines and husbandry

All zebrafish strains were maintained under standard husbandry conditions. The lines used in this study were: Wild type (AB), *plxnd1*^{fov01b} (Childs et al., 2002), *sema3aa*^{sa10241} and *sema3c* ^{sa15161} (Kettleborough et al., 2013), *Tg(lyve1b:EGFP)*^{nz150}, *Tg(lyve1b:DsRed)*^{nz101} (Okuda et al., 2012), *Tg(fli1a:EGFP)*^{y1} (Lawson and Weinstein, 2002), *Tg(fli1a:nlsEGFP)*^{y7} (Roman et al., 2002), *Tg(kdrl:EGFP)*^{s843}(Jin et al., 2005), *Tg(kdrl:nlsmCherry)*^{nz49} (Lam et al., 2010), *Tg(kdrl:RFP)*^{la4} (Huang et al., 2005), *Tg(prox1a:KalTA4)*^{uq3bh} ; *Tg(10xUAS: Venus)* - known as *prox1a:Venus* (Koltowska et al., 2015). *plxnd1*^{nz75} was generated in this study.

ENU Mutagenesis

ENU mutagenesis was performed as previously described (Solnica-Krezel et al., 1994). Briefly, *Tg(lyve1:DsRed)*^{nz101} males were mutagenised with weekly one hour exposures to 3 mM ENU (Sigma) over 5 weeks and crossed with wild type

lyve1:DsRed females to produce F1 families. Subsequent incrossing of F2 progeny generated F3 embryos that were screened for misguided lymphatics.

Identification of the *nz75* mutant by positional cloning

Genomic DNA from pooled *nz75* mutant larvae and wild type siblings (48 larvae each) was isolated using DNeasy Blood+Tissue kits (QIAGEN) and converted into libraries using the SureSelect^{XT} library preparation kit (Agilent Technologies) according to the manufacturer's instructions. Sequencing of libraries was performed on an Illumina NextSeq 500 with 150-bp paired-end reads. We obtained approximately 65 million reads per library.

The *nz75* mutation was then mapped using the raw fastq files with the SNPtrack algorithm (http://genetics.bwh.harvard.edu/snptrack/#) which maps the mutation to a genomic region by calculating the homozygosity score, expressed as a ratio of heterozygous SNP calls between wild type and mutant pools multiplied by the number of informative homozygous SNP calls in the mutant pool (Leshchiner et al., 2012).

RNA was extracted from both *plxnd1*^{nz75} mutant and wild type siblings and cDNA generated using random hexamer primers. Eight overlapping PCR products (see Supplementary Table 1 for primer sequences) within the coding region of *plxnd1* were generated, sequenced and aligned to the reference to identify the *nz75* mutation.

Genotyping *sema* mutants

sema3aa^{sa10241} and *sema3c* ^{sa15161} mutants were genotyped through the Sanger sequencing of genomic PCR products from whole larvae following imaging at 6 dpf (see Supplementary Table 1 for primer sequences).

Whole mount *in situ* hybridisation

In situ hybridisation for *plxnd1*, *egfp, sema3ab* and *sema3c* were performed on whole zebrafish larvae using the *in situ* HCR kit (Molecular Instruments) according to manufacturer's instructions (Choi et al., 2018). *In situ* hybridisation for *sema3aa* was performed as described previously (Jowett and Lettice, 1994) using a 717 bp antisense, digoxigenin-labeled (DIG-labeled) riboprobe (see supplemental table 1 for primer sequences used).

Morpholino injections

Morpholino injections were conducted as previously described (Nasevicius and Ekker, 2000). Morpholino sequences and doses are given in Supplementary Table 2. The *plxnd1* (Torres-Vazquez et al., 2004), and *vegfd* MOs (Astin et al., 2014a; Bower et al., 2017) have been previously validated by comparison to a corresponding null mutant allele as per field guidelines (Stainier et al., 2017).

Inhibitor treatments

The embryos were raised to 2 dpf (in order to assess the effect on the misguidance phenotype) or 3 dpf (in order to assess the effect on the overgrowth phenotype), and then placed in a solution of 0.5% DMSO, 2 nM Tivozanib (Aveo Pharmaceuticals), 1 μM Sunitinib (Sigma-Aldrich) or 5 μM SL327 (Abcam), and the larvae were maintained in this solution until 6 dpf.

Cell transplantation

Cell transplantation was performed on 3 hpf embryos after manually dechorionating them on an agar bed. *lyve1b:DsRed; kdrl:EGFP* donor and *fli1a:EGFP* recipient embryos were placed into the troughs of an agar bed that was made using a transplantation mould (Adaptive Science Tools). Cells in the donor embryo were removed from approximately 1/10th of the distance from the yolk sac to the animal pole using a borosilicate microinjection needle attached to an Eppendorf CellTram, and then 10 - 20 cells were transplanted into the same region of the blastula on the recipient embryo. Transplanted recipients were collected and maintained in E3 solution on an agar bed until 24 hpf, after which they were raised according to standard husbandry conditions. Successful grafts were identified by *lyve1:DsRed* expression and were imaged at 6 dpf.

Immunohistochemistry

Immunohistochemistry to detect pErk within the PCV and the facial lymphatics was performed on *lyve1b:EGFP* embryos using chicken anti-EGFP (Abcam) and rabbit anti-p44/42 MAPK (Cell Signaling Technology) antibodies as described previously (Okuda et al., 2018).

RT-PCR

Reverse transcription PCR (RT-PCR) was used to confirm the expression of *sema* genes. 22, 30 or 48 hpf larvae had their head and trunk tissue removed by dissection with a scalpel and total RNA was extracted. cDNA synthesis was conducted using random hexamer primers on 2 ug of total RNA before PCR with gene specific primers (see supplemental table 1 for primer sequences used).

Confocal live imaging of zebrafish

Embryos were imaged as described (Eng and Astin, 2018) with a Nikon D-Eclipse C1 confocal microscope or with an Olympus FV1000 confocal microscope for time-lapse microscopy. Still images were taken using Z stacks 5 µm apart. For time-lapse microscopy, Z stacks of 5 µm apart were taken at 15 minute intervals. Confocal images in this study are maximum projections of Z series stacks. Images were processed using ImageJ (NIH, Bethesda, MD, USA), Photoshop CS5 (Adobe, San Jose, CA, USA), and Volocity 5.4 image analysis software (Improvision/PerkinElmer Life and Analytical Sciences, Shelton, CT, USA).

Zebrafish image analysis and statistics

Thoracic duct formation was quantitated by live imaging *lyve1b:DsRed* larvae at 6 dpf and measuring the percentage of somites 7-17 containing a segment of TD (Astin et al., 2014a). Abberant facial lymphatics were identified as any branches not typically seen in the OLV, MFL and LFL as previously defined (Eng and Astin, 2018). Misaligned ISLVs were quantitated by live imaging *lyve1b:DsRed; kdrl:EGFP* or *lyve1b:DsRed; fli1a:EGFP* larvae at 6 dpf and counting any ISLVs that were not completely aligned with an ISV across somites 7-11. For grafted animals, quantitation was conducted in the regions containing donor cells as identified by *lyve1:DsRed* expressing cells. Facial LECs (Eng and Astin, 2018) and trunk LECs were quantitated as previously described (Okuda et al., 2018).

Aberrant ISVs were counted by live imaging *kdrl:EGFP* embryos at 48 hpf and identifying all the ISVs between somites 7-11 that could be seen just dorsal to the DA and then counting as aberrant those that did not arise from the DA at a position aligned with an intersomitic boundary. Artery:vein ratio was quantitated by live imaging *kdrl:EGFP* larvae at 3 dpf and identifying them as aISVs or vISVs based on their connection to the DA or PCV respectively. Secondary sprouts were counted between somites 7-11 by live imaging *lyve1b:EGFP* embryos at 36 hpf. Parachordal LEC formation was quantitated by live imaging *lyve1b:EGFP* larvae at 48 hpf and measuring the percentage of somites 7-17 containing a LEC(s) (Astin et al., 2014b).

ISLV time-lapse analysis was conducted by time-lapse imaging *lyve1b:DsRed; kdrl:EGFP* larvae from 50-75 hpf and identifying an ISLV that grows from the horizontal myoseptum and subsequently displayed 6 hours of growth for analysis. The

aISV contact percentage was calculated as the percentage of time that the ISLV was no more than 20 μm from an aISV. The meandering index was determined by dividing the total growth of the ISLV (including branches that later retracted) over the net migration distance and the number of branching events was counted for each ISLV to give branching events/hour.

Statistical analysis was performed using Prism 5.0 software (GraphPad Software Inc). Normality of distribution of data was identified by Shapiro-Wilks test. Significance of two sets of data was determined by Mann-Whitney or t-tests depending on whether the data was normally distributed. Significance across three or more sets of data was determined by One-way ANOVA or Kruskal-Wallis tests depending on whether the data was normally distributed. Welch's correction was performed if different variances were detected.

ACKNOWLEDGEMENTS

This work was supported by a project grants from the Health Research Council of New Zealand (14/105) and by Royal Society Marsden Grants (UOA1602 and 20-UOA-27) to J.W.A. S.K.B and P.M.K were supported by the Family of Marijana Kumerich and by Leukaemia & Blood Cancer New Zealand. Grants (5R01HL133687 and 1R01HL161090-01A1 to J.T-V) from the National Heart Lung and Blood Institute (NHLBI), National Institutes of Health (NIH, United States of America) supported the work by J.H and J.T-V. We thank Alhad Mahagaonkar for expert management of our zebrafish facility and the Biomedical Imaging Research Unit, School of Medical Sciences, University of Auckland and Yang Deng, Michael

Cammer and the NYU School of Medicine's Microscopy Laboratory (grant NCRR S10 RR024708) for assistance in confocal microscopy.

AUTHOR CONTRIBUTIONS

J.W.A, P.M.K, S.K.B, B.H.M, C.J.H, J.T-V conceived and planned the experiments and analysed the data. D.D.B, J.H, J.P.M, W.C, P.M.K, L.G, C.D.H, J.W.A performed the experiments. The manuscript was written by D.D.B, J.T-V and J.W.A. All authors reviewed and corrected the manuscript.

REFERENCES

Astin, J. W., Haggerty, M. J., Okuda, K. S., Le Guen, L., Misa, J. P., Tromp, A., Hogan, B. M., Crosier, K. E. and Crosier, P. S. (2014a). Vegfd can compensate for loss of Vegfc in zebrafish facial lymphatic sprouting. *Development* **141**, 2680-2690.

Astin, J. W., Jamieson, S. M., Eng, T. C., Flores, M. V., Misa, J. P., Chien, A., Crosier, K. E. and Crosier, P. S. (2014b). An in vivo antilymphatic screen in zebrafish identifies novel inhibitors of Mammalian lymphangiogenesis and lymphatic-mediated metastasis. *Mol Cancer Ther* **13**, 2450-2462.

Aurandt, J., Li, W. and Guan, K. L. (2006). Semaphorin 4D activates the MAPK pathway downstream of plexin-B1. *Biochem J* **394**, 459-464.

Baek, S., Oh, T. G., Secker, G., Sutton, D. L., Okuda, K. S., Paterson, S., Bower, N. I., Toubia, J., Koltowska, K., Capon, S. J., et al. (2019). The Alternative Splicing Regulator Nova2 Constrains Vascular Erk Signaling to Limit Specification of the Lymphatic Lineage. *Dev Cell* **49**, 279-292 e275.

Basile, J. R., Gavard, J. and Gutkind, J. S. (2007). Plexin-B1 utilizes RhoA and Rho kinase to promote the integrin-dependent activation of Akt and ERK and endothelial cell motility. *J Biol Chem* **282**, 34888-34895.

Bower, N. I., Vogrin, A. J., Le Guen, L., Chen, H., Stacker, S. A., Achen, M. G. and Hogan, B. M. (2017). Vegfd modulates both angiogenesis and lymphangiogenesis during zebrafish embryonic development. *Development* **144**, 507-518.

Bribian, A., Nocentini, S., Llorens, F., Gil, V., Mire, E., Reginensi, D., Yoshida, Y., Mann, F. and del Rio, J. A. (2014). Sema3E/PlexinD1 regulates the migration of hem-derived Cajal-Retzius cells in developing cerebral cortex. *Nat Commun* **5**, 4265.

Brouillard, P., Witte, M. H., Erickson, R. P., Damstra, R. J., Becker, C., Quere, I. and Vikkula, M. (2021). Primary lymphoedema. *Nat Rev Dis Primers* **7**, 77.

Burk, K., Mire, E., Bellon, A., Hocine, M., Guillot, J., Moraes, F., Yoshida, Y., Simons, M., Chauvet, S. and Mann, F. (2017). Post-endocytic sorting of Plexin-D1 controls signal transduction and development of axonal and vascular circuits. *Nat Commun* **8**, 14508.

Bussmann, J., Bos, F. L., Urasaki, A., Kawakami, K., Duckers, H. J. and Schulte-Merker, S. (2010). Arteries provide essential guidance cues for

lymphatic endothelial cells in the zebrafish trunk. *Development* **137**, 2653-2657.

Callander, D. C., Lamont, R. E., Childs, S. J. and McFarlane, S. (2007). Expression of multiple class three semaphorins in the retina and along the path of zebrafish retinal axons. *Dev Dyn* **236**, 2918-2924.

Carretero-Ortega, J., Chhangawala, Z., Hunt, S., Narvaez, C., Menendez-Gonzalez, J., Gay, C. M., Zygmunt, T., Li, X. and Torres-Vazquez, J. (2019). GIPC proteins negatively modulate Plexind1 signaling during vascular development. *Elife* **8**.

Cha, Y. R., Fujita, M., Butler, M., Isogai, S., Kochhan, E., Siekmann, A. F. and Weinstein, B. M. (2012). Chemokine signaling directs trunk lymphatic network formation along the preexisting blood vasculature. *Dev Cell* **22**, 824-836.

Childs, S., Chen, J. N., Garrity, D. M. and Fishman, M. C. (2002). Patterning of angiogenesis in the zebrafish embryo. *Development* **129**, 973-982.

Choi, H. M. T., Schwarzkopf, M., Fornace, M. E., Acharya, A., Artavanis, G., Stegmaier, J., Cunha, A. and Pierce, N. A. (2018). Third-generation in situ hybridization chain reaction: multiplexed, quantitative, sensitive, versatile, robust. *Development* **145**.

Choi, Y. I., Duke-Cohan, J. S., Chen, W., Liu, B., Rossy, J., Tabarin, T., Ju, L., Gui, J., Gaus, K., Zhu, C., et al. (2014). Dynamic control of beta1 integrin adhesion by the plexinD1-sema3E axis. *Proc Natl Acad Sci U S A* **111**, 379-384.

Coso, S., Zeng, Y., Opeskin, K. and Williams, E. D. (2012). Vascular endothelial growth factor receptor-3 directly interacts with phosphatidylinositol 3-kinase to regulate lymphangiogenesis. *PLoS One* **7**, e39558.

Dashkevich, A., Raissadati, A., Syrjala, S. O., Zarkada, G., Keranen, M. A., Tuuminen, R., Krebs, R., Anisimov, A., Jeltsch, M., Leppanen, V. M., et al. (2016). Ischemia-Reperfusion Injury Enhances Lymphatic Endothelial VEGFR3 and Rejection in Cardiac Allografts. *Am J Transplant* **16**, 1160-1172.

Deng, Y., Zhang, X. and Simons, M. (2015). Molecular controls of lymphatic VEGFR3 signaling. *Arterioscler Thromb Vasc Biol* **35**, 421-429.

Dieterich, L. C. and Detmar, M. (2015). Tumor lymphangiogenesis and new drug development. *Adv Drug Deliv Rev*.

Dietrich, T., Bock, F., Yuen, D., Hos, D., Bachmann, B. O., Zahn, G., Wiegand, S., Chen, L. and Cursiefen, C. (2010). Cutting edge: lymphatic vessels, not blood vessels, primarily mediate immune rejections after transplantation. *J Immunol* **184**, 535-539.

Driessens, M. H., Hu, H., Nobes, C. D., Self, A., Jordens, I., Goodman, C. S. and Hall, A. (2001). Plexin-B semaphorin receptors interact directly with active Rac and regulate the actin cytoskeleton by activating Rho. *Curr Biol* **11**, 339-344.

Eng, T. C., Chen, W., Okuda, K. S., Misa, J. P., Padberg, Y., Crosier, K. E., Crosier, P. S., Hall, C. J., Schulte-Merker, S., Hogan, B. M., et al. (2019). Zebrafish facial lymphatics develop through sequential addition of venous and non-venous progenitors. *EMBO Rep* **20**.

Eng, T. C. Y. and Astin, J. W. (2018). Characterization of Zebrafish Facial Lymphatics. *Methods Mol Biol* **1846**, 71-83.

Fukushima, Y., Okada, M., Kataoka, H., Hirashima, M., Yoshida, Y., Mann, F., Gomi, F., Nishida, K., Nishikawa, S. and Uemura, A. (2011). Sema3E-PlexinD1 signaling selectively suppresses disoriented angiogenesis in ischemic retinopathy in mice. *J Clin Invest* **121**, 1974-1985.

Gay, C. M., Zygmunt, T. and Torres-Vazquez, J. (2011). Diverse functions for the semaphorin receptor PlexinD1 in development and disease. *Dev Biol* **349**, 1-19.

Geudens, I., Coxam, B., Alt, S., Gebala, V., Vion, A. C., Meier, K., Rosa, A. and Gerhardt, H. (2019). Artery-vein specification in the zebrafish trunk is pre-patterned by heterogeneous Notch activity and balanced by flow-mediated fine-tuning. *Development* **146**.

Geudens, I., Herpers, R., Hermans, K., Segura, I., Ruiz de Almodovar, C., Bussmann, J., De Smet, F., Vandevelde, W., Hogan, B. M., Siekmann, A., et al. (2010). Role of delta-like-4/Notch in the formation and wiring of the lymphatic network in zebrafish. *Arterioscler Thromb Vasc Biol* **30**, 1695-1702.

Gitler, A. D., Lu, M. M. and Epstein, J. A. (2004). PlexinD1 and semaphorin signaling are required in endothelial cells for cardiovascular development. *Dev Cell* **7**, 107-116.

Gousopoulos, E., Proulx, S. T., Bachmann, S. B., Dieterich, L. C., Scholl, J., Karaman, S., Bianchi, R. and Detmar, M. (2017). An Important Role of VEGF-C in Promoting Lymphedema Development. *J Invest Dermatol* **137**, 1995-2004.

Grimm, L., Nakajima, H., Chaudhury, S., Bower, N. I., Okuda, K. S., Cox, A. G., Harvey, N. L., Koltowska, K., Mochizuki, N. and Hogan, B. M. (2019). Yap1 promotes sprouting and proliferation of lymphatic progenitors downstream of Vegfc in the zebrafish trunk. *Elife* **8**.

Gu, C., Yoshida, Y., Livet, J., Reimert, D. V., Mann, F., Merte, J., Henderson, C. E., Jessell, T. M., Kolodkin, A. L. and Ginty, D. D. (2005). Semaphorin 3E and plexin-D1 control vascular pattern independently of neuropilins. *Science* **307**, 265-268.

Hagerling, R., Pollmann, C., Andreas, M., Schmidt, C., Nurmi, H., Adams, R. H., Alitalo, K., Andresen, V., Schulte-Merker, S. and Kiefer, F. (2013). A novel multistep mechanism for initial lymphangiogenesis in mouse embryos based on ultramicroscopy. *EMBO J* **32**, 629-644.

Hamm, M. J., Kirchmaier, B. C. and Herzog, W. (2016). Sema3d controls collective endothelial cell migration by distinct mechanisms via Nrp1 and PlxnD1. *J Cell Biol* **215**, 415-430.

Hogan, B. M., Bos, F. L., Bussmann, J., Witte, M., Chi, N. C., Duckers, H. J. and Schulte-Merker, S. (2009a). Ccbe1 is required for embryonic lymphangiogenesis and venous sprouting. *Nat Genet* **41**, 396-398.

Hogan, B. M., Herpers, R., Witte, M., Helotera, H., Alitalo, K., Duckers, H. J. and Schulte-Merker, S. (2009b). Vegfc/Flt4 signalling is suppressed by Dll4 in developing zebrafish intersegmental arteries. *Development* **136**, 4001-4009.

Huang, H., Zhang, B., Hartenstein, P. A., Chen, J. N. and Lin, S. (2005). NXT2 is required for embryonic heart development in zebrafish. *BMC Dev Biol* **5**, 7.

Ishii, E., Shimizu, A., Kuwahara, N., Arai, T., Kataoka, M., Wakamatsu, K., Ishikawa, A., Nagasaka, S. and Fukuda, Y. (2010). Lymphangiogenesis

associated with acute cellular rejection in rat liver transplantation. *Transplant Proc* **42**, 4282-4285.

Isogai, S., Lawson, N. D., Torrealday, S., Horiguchi, M. and Weinstein, B. M. (2003). Angiogenic network formation in the developing vertebrate trunk. *Development* **130**, 5281-5290.

Ito, T., Morita, T., Yoshida, K., Negishi, T. and Yukawa, K. (2014). Semaphorin 3A-Plexin-A1 signaling through ERK activation is crucial for Toll-like receptor-induced NO production in BV-2 microglial cells. *Int J Mol Med* **33**, 1635-1642.

Jin, S. W., Beis, D., Mitchell, T., Chen, J. N. and Stainier, D. Y. (2005). Cellular and molecular analyses of vascular tube and lumen formation in zebrafish. *Development* **132**, 5199-5209.

Jowett, T. and Lettice, L. (1994). Whole-mount in situ hybridizations on zebrafish embryos using a mixture of digoxigenin- and fluorescein-labelled probes. *Trends Genet* **10**, 73-74.

Jung, H. M., Castranova, D., Swift, M. R., Pham, V. N., Venero Galanternik, M., Isogai, S., Butler, M. G., Mulligan, T. S. and Weinstein, B. M. (2017). Development of the larval lymphatic system in zebrafish. *Development* **144**, 2070-2081.

Karkkainen, M. J., Haiko, P., Sainio, K., Partanen, J., Taipale, J., Petrova, T. V., Jeltsch, M., Jackson, D. G., Talikka, M., Rauvala, H., et al. (2004). Vascular endothelial growth factor C is required for sprouting of the first lymphatic vessels from embryonic veins. *Nat Immunol* **5**, 74-80.

Kettleborough, R. N., Busch-Nentwich, E. M., Harvey, S. A., Dooley, C. M., de Bruijn, E., van Eeden, F., Sealy, I., White, R. J., Herd, C., Nijman, I. J., et al. (2013). A systematic genome-wide analysis of zebrafish protein-coding gene function. *Nature* **496**, 494-497.

Kim, J., Oh, W. J., Gaiano, N., Yoshida, Y. and Gu, C. (2011). Semaphorin 3E-Plexin-D1 signaling regulates VEGF function in developmental angiogenesis via a feedback mechanism. *Genes Dev* **25**, 1399-1411.

Koltowska, K., Lagendijk, A. K., Pichol-Thievend, C., Fischer, J. C., Francois, M., Ober, E. A., Yap, A. S. and Hogan, B. M. (2015). Vegfc Regulates Bipotential Precursor Division and Prox1 Expression to Promote Lymphatic Identity in Zebrafish. *Cell Rep* **13**, 1828-1841.

Krueger, J., Liu, D., Scholz, K., Zimmer, A., Shi, Y., Klein, C., Siekmann, A., Schulte-Merker, S., Cudmore, M., Ahmed, A., et al. (2011). Flt1 acts as a negative regulator of tip cell formation and branching morphogenesis in the zebrafish embryo. *Development* **138**, 2111-2120.

Kuchler, A. M., Gjini, E., Peterson-Maduro, J., Cancilla, B., Wolburg, H. and Schulte-Merker, S. (2006). Development of the zebrafish lymphatic system requires VEGFC signaling. *Curr Biol* **16**, 1244-1248.

Lam, E. Y., Hall, C. J., Crosier, P. S., Crosier, K. E. and Flores, M. V. (2010). Live imaging of Runx1 expression in the dorsal aorta tracks the emergence of blood progenitors from endothelial cells. *Blood* **116**, 909-914.

Lawson, N. D. and Weinstein, B. M. (2002). In vivo imaging of embryonic vascular development using transgenic zebrafish. *Dev Biol* **248**, 307-318.

Leshchiner, I., Alexa, K., Kelsey, P., Adzhubei, I., Austin-Tse, C. A., Cooney, J. D., Anderson, H., King, M. J., Stottmann, R. W., Garnaas, M. K., et al.

(2012). Mutation mapping and identification by whole-genome sequencing. *Genome Res* **22**, 1541-1548.

Lim, A. H., Suli, A., Yaniv, K., Weinstein, B., Li, D. Y. and Chien, C. B. (2011). Motoneurons are essential for vascular pathfinding. *Development* **138**, 3847-3857.

Liu, X., Uemura, A., Fukushima, Y., Yoshida, Y. and Hirashima, M. (2016). Semaphorin 3G Provides a Repulsive Guidance Cue to Lymphatic Endothelial Cells via Neuropilin-2/PlexinD1. *Cell Rep* **17**, 2299-2311.

Maruyama, K., Naemura, K., Arima, Y., Uchijima, Y., Nagao, H., Yoshihara, K., Singh, M. K., Uemura, A., Matsuzaki, F., Yoshida, Y., et al. (2021). Semaphorin3E-PlexinD1 signaling in coronary artery and lymphatic vessel development with clinical implications in myocardial recovery. *iScience* **24**, 102305.

Moriya, J., Minamino, T., Tateno, K., Okada, S., Uemura, A., Shimizu, I., Yokoyama, M., Nojima, A., Okada, M., Koga, H., et al. (2010). Inhibition of semaphorin as a novel strategy for therapeutic angiogenesis. *Circ Res* **106**, 391-398.

Nasevicius, A. and Ekker, S. C. (2000). Effective targeted gene 'knockdown' in zebrafish. *Nat Genet* **26**, 216-220.

Nicenboim, J., Malkinson, G., Lupo, T., Asaf, L., Sela, Y., Mayseless, O., Gibbs-Bar, L., Senderovich, N., Hashimshony, T., Shin, M., et al. (2015). Lymphatic vessels arise from specialized angioblasts within a venous niche. *Nature* **522**, 56-61.

Okuda, K. S., Astin, J. W., Misa, J. P., Flores, M. V., Crosier, K. E. and Crosier, P. S. (2012). lyve1 expression reveals novel lymphatic vessels and new mechanisms for lymphatic vessel development in zebrafish. *Development* **139**, 2381-2391.

Okuda, K. S., Baek, S. and Hogan, B. M. (2018). Visualization and Tools for Analysis of Zebrafish Lymphatic Development. *Methods Mol Biol* **1846**, 55-70.

Okuda, K. S., Misa, J. P., Oehlers, S. H., Hall, C. J., Ellett, F., Alasmari, S., Lieschke, G. J., Crosier, K. E., Crosier, P. S. and Astin, J. W. (2015). A zebrafish model of inflammatory lymphangiogenesis. *Biol Open* **4**, 1270-1280.

Pedersen, M. S., Muller, M., Rulicke, T., Leitner, N., Kain, R., Regele, H., Wang, S., Grone, H. J., Rong, S., Haller, H., et al. (2020). Lymphangiogenesis in a mouse model of renal transplant rejection extends life span of the recipients. *Kidney Int* **97**, 89-94.

Peng, D., Ando, K., Hussmann, M., Gloger, M., Skoczylas, R., Mochizuki, N., Betsholtz, C., Fukuhara, S., Schulte-Merker, S., Lawson, N. D., et al. (2022). Proper migration of lymphatic endothelial cells requires survival and guidance cues from arterial mural cells. *Elife* **11**.

Roman, B. L., Pham, V. N., Lawson, N. D., Kulik, M., Childs, S., Lekven, A. C., Garrity, D. M., Moon, R. T., Fishman, M. C., Lechleider, R. J., et al. (2002). Disruption of acvrl1 increases endothelial cell number in zebrafish cranial vessels. *Development* **129**, 3009-3019.

Saito, Y., Nakagami, H., Kaneda, Y. and Morishita, R. (2013). Lymphedema and therapeutic lymphangiogenesis. *Biomed Res Int* **2013**, 804675.

Sakurai, A., Gavard, J., Annas-Linhares, Y., Basile, J. R., Amornphimoltham, P., Palmby, T. R., Yagi, H., Zhang, F., Randazzo, P. A., Li, X., et al. (2010). Semaphorin 3E initiates antiangiogenic signaling through plexin D1 by regulating Arf6 and R-Ras. *Mol Cell Biol* **30**, 3086-3098.

Sakurai, A., Jian, X., Lee, C. J., Manavski, Y., Chavakis, E., Donaldson, J., Randazzo, P. A. and Gutkind, J. S. (2011). Phosphatidylinositol-4-phosphate 5-kinase and GEP100/Brag2 protein mediate antiangiogenic signaling by semaphorin 3E-plexin-D1 through Arf6 protein. *J Biol Chem* **286**, 34335-34345.

Salameh, A., Galvagni, F., Bardelli, M., Bussolino, F. and Oliviero, S. (2005). Direct recruitment of CRK and GRB2 to VEGFR-3 induces proliferation, migration, and survival of endothelial cells through the activation of ERK, AKT, and JNK pathways. *Blood* **106**, 3423-3431.

Shin, M., Male, I., Beane, T. J., Villefranc, J. A., Kok, F. O., Zhu, L. J. and Lawson, N. D. (2016). Vegfc acts through ERK to induce sprouting and differentiation of trunk lymphatic progenitors. *Development* **143**, 3785-3795.

Solnica-Krezel, L., Schier, A. F. and Driever, W. (1994). Efficient recovery of ENU-induced mutations from the zebrafish germline. *Genetics* **136**, 1401-1420.

Srinivasan, R. S., Dillard, M. E., Lagutin, O. V., Lin, F. J., Tsai, S., Tsai, M. J., Samokhvalov, I. M. and Oliver, G. (2007). Lineage tracing demonstrates the venous origin of the mammalian lymphatic vasculature. *Genes Dev* **21**, 2422-2432.

Stacker, S. A., Williams, S. P., Karnezis, T., Shayan, R., Fox, S. B. and Achen, M. G. (2014). Lymphangiogenesis and lymphatic vessel remodelling in cancer. *Nat Rev Cancer* **14**, 159-172.

Stainier, D. Y. R., Raz, E., Lawson, N. D., Ekker, S. C., Burdine, R. D., Eisen, J. S., Ingham, P. W., Schulte-Merker, S., Yelon, D., Weinstein, B. M., et al. (2017). Guidelines for morpholino use in zebrafish. *PLoS Genet* **13**, e1007000.

Tanaka, H., Maeda, R., Shoji, W., Wada, H., Masai, I., Shiraki, T., Kobayashi, M., Nakayama, R. and Okamoto, H. (2007). Novel mutations affecting axon guidance in zebrafish and a role for plexin signalling in the guidance of trigeminal and facial nerve axons. *Development* **134**, 3259-3269.

Tata, A., Stoppel, D. C., Hong, S., Ben-Zvi, A., Xie, T. and Gu, C. (2014). An image-based RNAi screen identifies SH3BP1 as a key effector of Semaphorin 3E-PlexinD1 signaling. *J Cell Biol* **205**, 573-590.

Torres-Vazquez, J., Gitler, A. D., Fraser, S. D., Berk, J. D., Van, N. P., Fishman, M. C., Childs, S., Epstein, J. A. and Weinstein, B. M. (2004). Semaphorin-plexin signaling guides patterning of the developing vasculature. *Dev Cell* **7**, 117-123.

Toyofuku, T., Yabuki, M., Kamei, J., Kamei, M., Makino, N., Kumanogoh, A. and Hori, M. (2007). Semaphorin-4A, an activator for T-cell-mediated immunity, suppresses angiogenesis via Plexin-D1. *EMBO J* **26**, 1373-1384.

Uesugi, K., Oinuma, I., Katoh, H. and Negishi, M. (2009). Different requirement for Rnd GTPases of R-Ras GAP activity of Plexin-C1 and Plexin-D1. *J Biol Chem* **284**, 6743-6751.

Vivekanandhan, S., Madamsetty, V. S., Angom, R. S., Dutta, S. K., Wang, E., Caulfield, T., Pletnev, A. A., Upstill-Goddard, R., Asmann, Y. W., Chang, D., et al. (2021). Role of PLEXIND1/TGFbeta Signaling Axis in Pancreatic Ductal Adenocarcinoma Progression Correlates with the Mutational Status of KRAS. *Cancers (Basel)* **13**.

Vogrin, A. J., Bower, N. I., Gunzburg, M. J., Roufail, S., Okuda, K. S., Paterson, S., Headey, S. J., Stacker, S. A., Hogan, B. M. and Achen, M. G. (2019). Evolutionary Differences in the Vegf/Vegfr Code Reveal Organotypic Roles for the Endothelial Cell Receptor Kdr in Developmental Lymphangiogenesis. *Cell Rep* **28**, 2023-2036 e2024.

Wang, G., Muhl, L., Padberg, Y., Dupont, L., Peterson-Maduro, J., Stehling, M., le Noble, F., Colige, A., Betsholtz, C., Schulte-Merker, S., et al. (2020). Specific fibroblast subpopulations and neuronal structures provide local sources of Vegfc-processing components during zebrafish lymphangiogenesis. *Nat Commun* **11**, 2724.

Wang, Y., He, H., Srivastava, N., Vikarunnessa, S., Chen, Y. B., Jiang, J., Cowan, C. W. and Zhang, X. (2012). Plexins are GTPase-activating proteins for Rap and are activated by induced dimerization. *Sci Signal* **5**, ra6.

Wigle, J. T., Harvey, N., Detmar, M., Lagutina, I., Grosveld, G., Gunn, M. D., Jackson, D. G. and Oliver, G. (2002). An essential role for Prox1 in the induction of the lymphatic endothelial cell phenotype. *EMBO J* **21**, 1505-1513.

Wigle, J. T. and Oliver, G. (1999). Prox1 function is required for the development of the murine lymphatic system. *Cell* **98**, 769-778.

Wild, R., Klems, A., Takamiya, M., Hayashi, Y., Strahle, U., Ando, K., Mochizuki, N., van Impel, A., Schulte-Merker, S., Krueger, J., et al. (2017). Neuronal sFlt1 and Vegfaa determine venous sprouting and spinal cord vascularization. *Nat Commun* **8**, 13991.

Wong, B. W. (2020). Lymphatic vessels in solid organ transplantation and immunobiology. *Am J Transplant* **20**, 1992-2000.

Wortzel, I. and Seger, R. (2011). The ERK Cascade: Distinct Functions within Various Subcellular Organelles. *Genes Cancer* **2**, 195-209.

Yang, W. J., Hu, J., Uemura, A., Tetzlaff, F., Augustin, H. G. and Fischer, A. (2015). Semaphorin-3C signals through Neuropilin-1 and PlexinD1 receptors to inhibit pathological angiogenesis. *EMBO Mol Med* **7**, 1267-1284.

Yang, Y., Garcia-Verdugo, J. M., Soriano-Navarro, M., Srinivasan, R. S., Scallan, J. P., Singh, M. K., Epstein, J. A. and Oliver, G. (2012). Lymphatic endothelial progenitors bud from the cardinal vein and intersomitic vessels in mammalian embryos. *Blood* **120**, 2340-2348.

Yaniv, K., Isogai, S., Castranova, D., Dye, L., Hitomi, J. and Weinstein, B. M. (2006). Live imaging of lymphatic development in the zebrafish. *Nat Med* **12**, 711-716.

Yoon, Y. S., Murayama, T., Gravereaux, E., Tkebuchava, T., Silver, M., Curry, C., Wecker, A., Kirchmair, R., Hu, C. S., Kearney, M., et al. (2003). VEGF-C gene therapy augments postnatal lymphangiogenesis and ameliorates secondary lymphedema. *J Clin Invest* **111**, 717-725.

Yu, H. H. and Moens, C. B. (2005). Semaphorin signaling guides cranial neural crest cell migration in zebrafish. *Dev Biol* **280**, 373-385.

Zhang, Y., Singh, M. K., Degenhardt, K. R., Lu, M. M., Bennett, J., Yoshida, Y. and Epstein, J. A. (2009). Tie2Cre-mediated inactivation of plexinD1 results in congenital heart, vascular and skeletal defects. *Dev Biol* **325**, 82-93.

Zhang, Y. F., Zhang, Y., Jia, D. D., Yang, H. Y., Cheng, M. D., Zhu, W. X., Xin, H., Li, P. F. and Zhang, Y. F. (2021). Insights into the regulatory role of Plexin D1 signalling in cardiovascular development and diseases. *J Cell Mol Med* **25**, 4183-4194.

Zhou, Y. F., Li, P. C., Wu, J. H., Haslam, J. A., Mao, L., Xia, Y. P., He, Q. W., Wang, X. X., Lei, H., Lan, X. L., et al. (2018). Sema3E/PlexinD1 inhibition is a therapeutic strategy for improving cerebral perfusion and restoring functional loss after stroke in aged rats. *Neurobiol Aging* **70**, 102-116.

Zygmunt, T., Gay, C. M., Blondelle, J., Singh, M. K., Flaherty, K. M., Means, P. C., Herwig, L., Krudewig, A., Belting, H. G., Affolter, M., et al. (2011). Semaphorin-PlexinD1 signaling limits angiogenic potential via the VEGF decoy receptor sFlt1. *Dev Cell* **21**, 301-314.

Figures

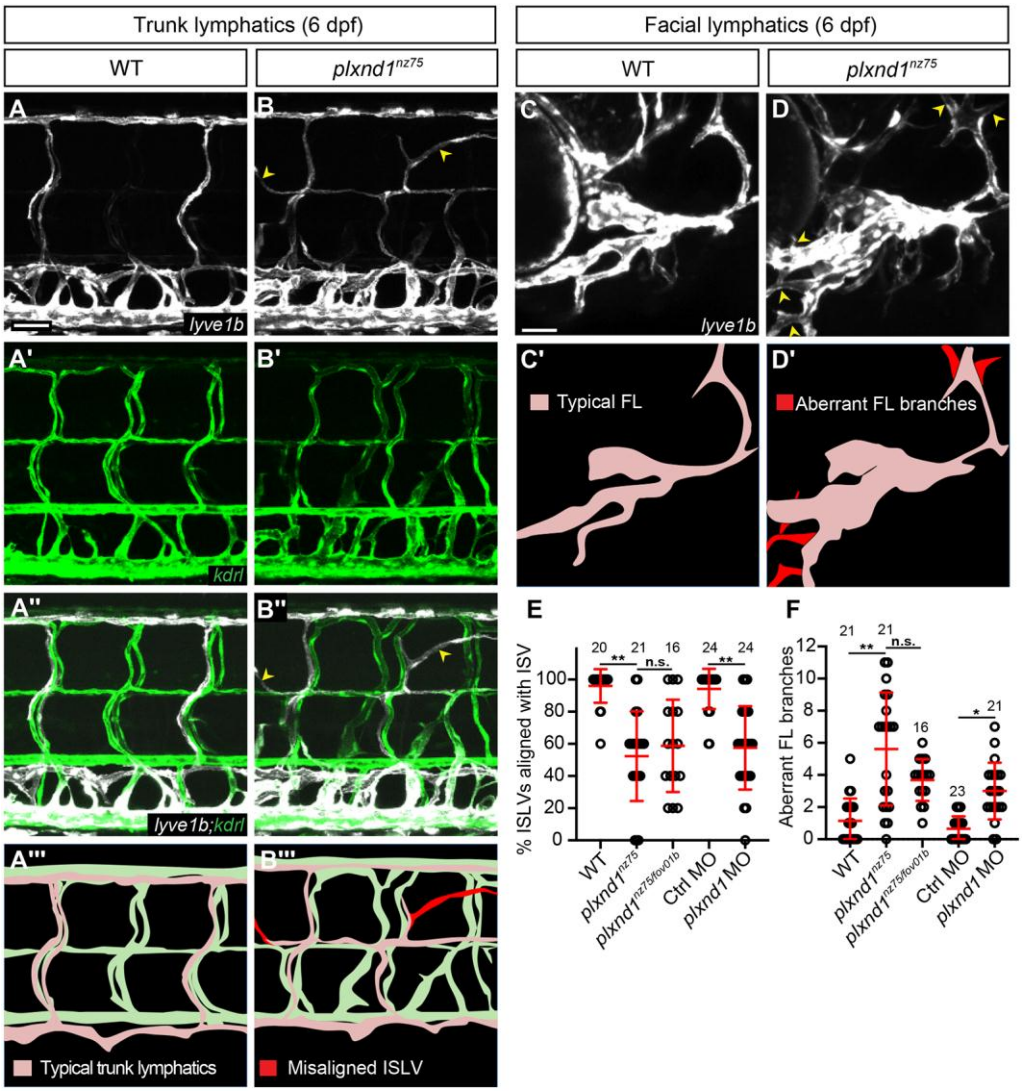

Fig. 1. *plxnd1* mutants have misaligned ISLVs and aberrant facial lymphatic branches

(**A-D)** Confocal images of the trunk (A-B) and facial (C-D) lymphatics in *lyve1b:DsRed* (white)*; kdrl:EGFP* (green) larvae at 6 dpf. Yellow arrowheads indicate ISLVs that are not aligned with an ISV (B) or aberrant facial lymphatic branches (D) in *plxnd1*^{nz75} larvae. *EGFP* vessels in the head not displayed for clarity. Schematics highlighting the misaligned ISLVs (A′′′-B′′′) or aberrant facial lymphatics

(C′-D′) in each corresponding confocal image. (**E-F**) Quantitation of the number of misaligned ISLVs (E) and aberrant facial lymphatic branches (F). n.s $p > 0.05$, * $p < 0.05$, ** $p < 0.01$, by Brown-Forsythe and Welch ANOVA and Kruskal-Wallis test; error bars indicate s.d. Scale bars: 50 μm. ISLV = intersegmental lymphatic vessel. Numbers in graphs represent numbers of larvae.

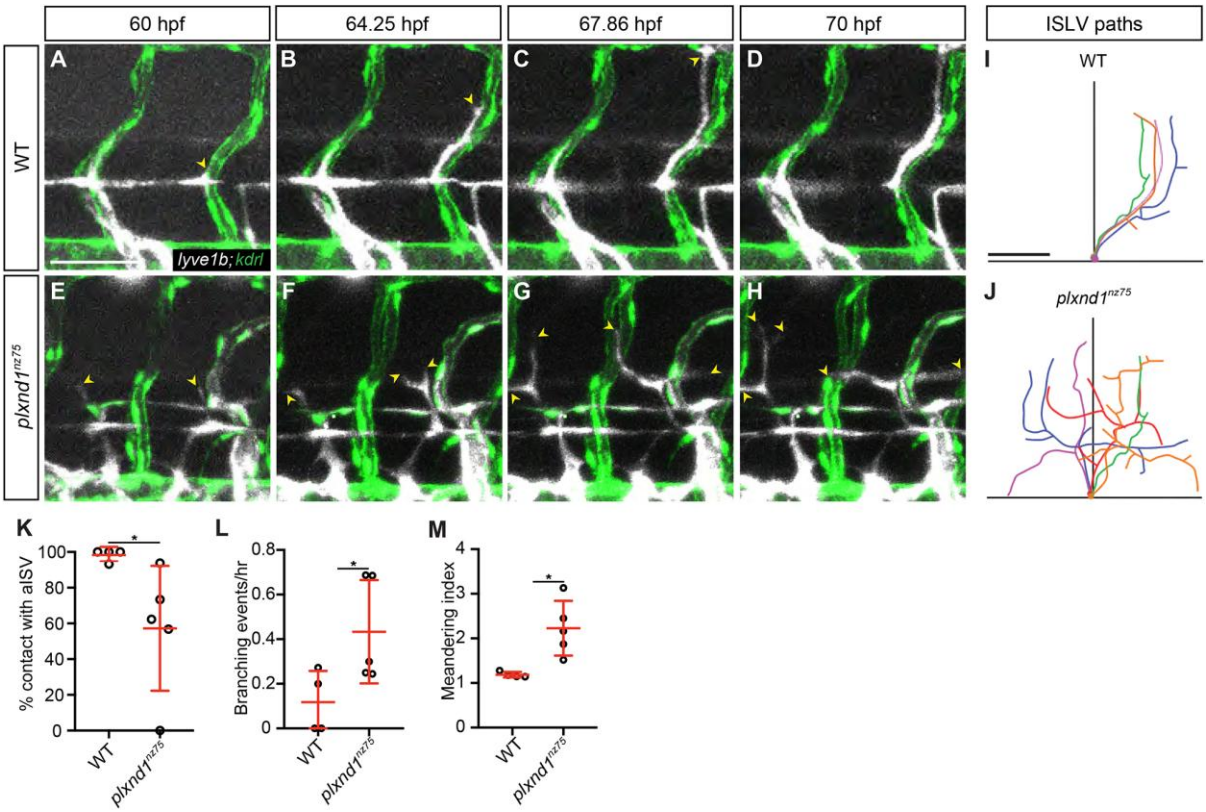

Fig. 2. *plxnd1* is required for the alignment of developing ISLVs to blood vessels

(A-H) Still images from time-lapse movies of ISLV growth between 60 to 70 hpf in *lyve1b:DsRed; kdrl:EGFP* wild type (A-D) and *plxnd1*^{nz75} (E-H) larvae showing blood vessels (green) *lyve1b*-expressing vessels (white) from Movies 1 and 2, respectively. Yellow arrowheads indicate the distal tip of each ISLV. **(I-J)** Traces of ISLV growth paths for wild type (I) and *plxnd1* (J) (n = 4). ISLVs were traced dorsally from when they left the horizontal myoseptum. **(K)** Quantitation of the percentage of time the ISLVs are aligned with a blood vessel (n = 4). **(L)** Quantitation of the number of ISLV branching events (n = 4). **(M)** Quantitation of the ISLV meandering index (n = 4). * p< 0.05, by Mann-Whitney test; error bars indicate s.d. Scale bars: 50 μm. ISLV = intersegmental lymphatic vessel.

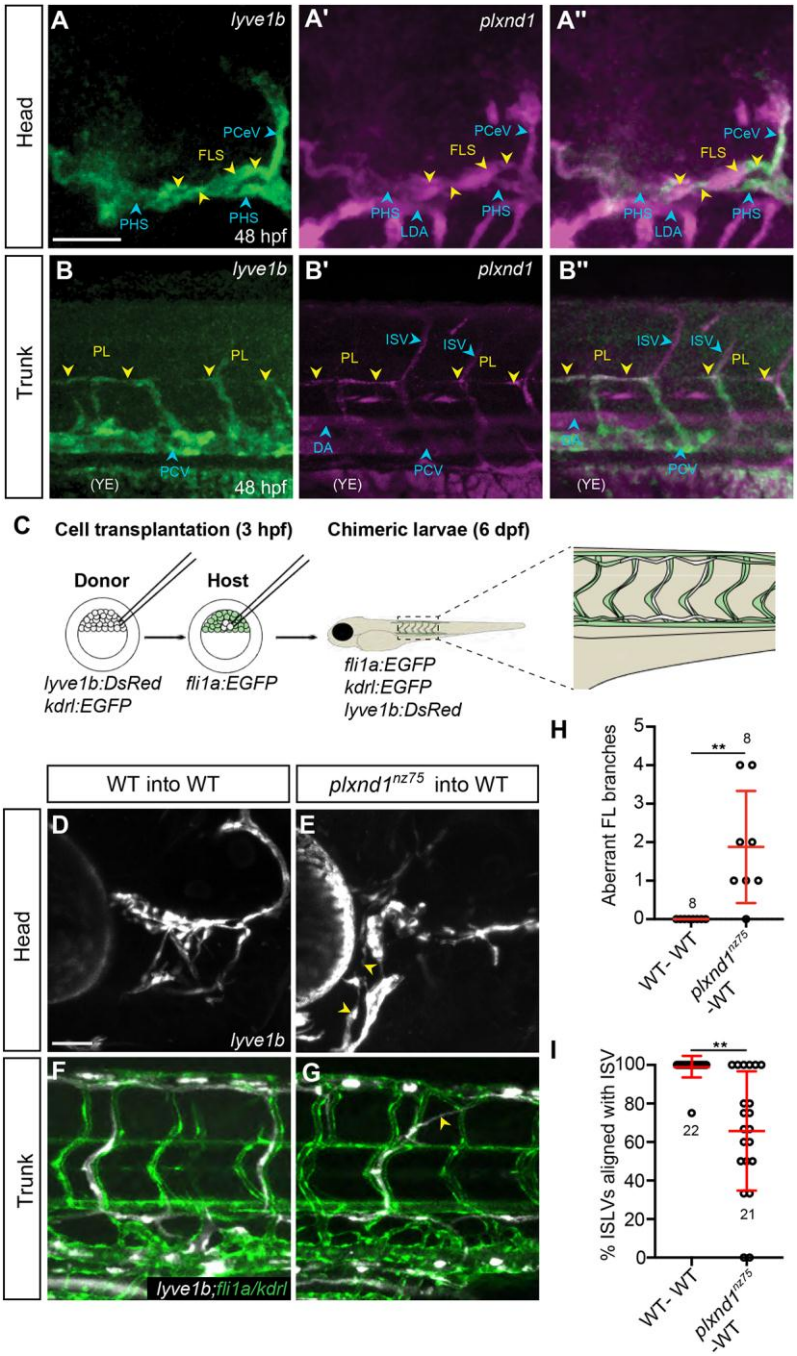

Fig. 3. *plxnd1* acts cell autonomously to guide lymphatic vessel growth

(**A-B)** Confocal images of the *lyve1b:EGFP* expression (anti-*EGFP* - green) (A, B), *plxnd1* expression (anti-*plxnd1* – magenta) (A′-B′) or both (A′′-B′′) in the head (A) or trunk (B) of 48 hpf *lyve1b:EGFP* larvae. Yellow arrowheads indicate either the facial

lymphatic sprout (A) or the parachordal LECs (B). Blue arrowheads indicate blood vessels. Note the non-specific staining in the yolk extension (YE). (**C**) Schematic of the transplantation protocol. Cells were transplanted from 3 hpf *lyve1b:DsRed; kdrl:EGFP* donor embryos to 3 hpf *fli1a:EGFP* host embryos resulting in chimeric larva with host-derived blood and lymphatic vessels indicated in light green and donor-derived lymphatic vessels indicated in white. **(D-E)** Confocal images of the facial vasculature in chimeric animals at 6 dpf showing donor-derived LECs (white) from either wild type (D) or *plxnd1*^{nz75} (E) donors. *EGFP* vessels not displayed for clarity. Aberrant *plxnd1*^{nz75} facial lymphatic vessels are highlighted by yellow arrowheads in E. **(F-G)** Confocal images of the trunk vasculature in chimeric animals at 6 dpf showing donor-derived LECs (white) from either wild type (F) or *plxnd1*^{nz75} (G) donors. Note the misaligned *plxnd1*^{nz75} vessel highlighted by the yellow arrowhead in G. **(H-I)** Quantitation of aberrant facial lymphatics (H) or the number of misaligned ISLVs (I) at 6 dpf. ** $p < 0.01$, by Mann-Whitney test; error bars indicate s.d. Scale bars: 50 μm. DA = dorsal aorta, FLS = facial lymphatic sprout, ISV = intersegmental vessel, ISLV = intersegmental lymphatic vessel, LDA = lateral dorsal aorta, PCV = posterior cardinal vein, PCeV = posterior cerebral vein, PL = parachordal LEC, PHS = primary head sinus, YE = yolk extension. Numbers in graphs represent numbers of larvae.

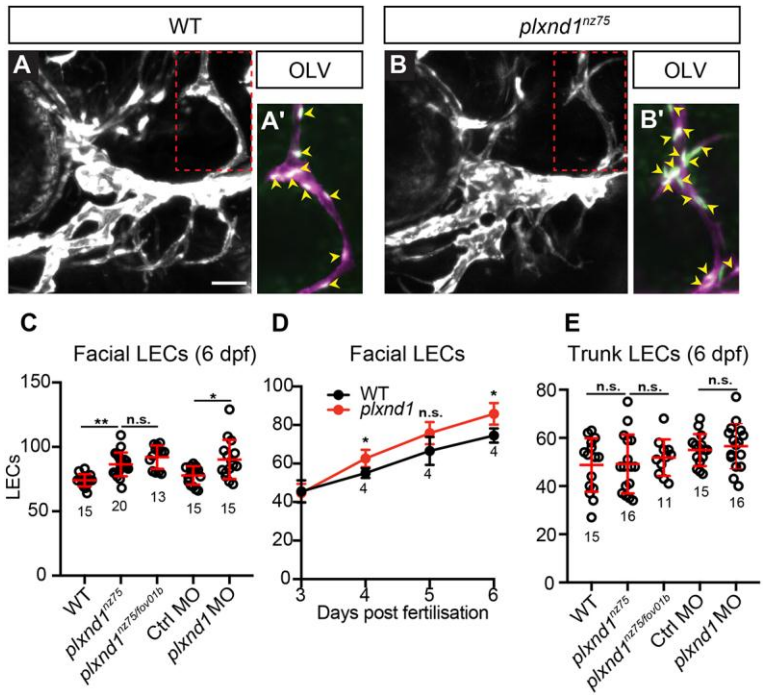

Fig. 4. *plxnd1* mutants display facial lymphatic hyperplasia

(A-B) Confocal images of the facial vasculature showing the *lyve1b*-expressing vessels (white) in 6 dpf *lyve1b:DsRed; fli1a:nlsEGFP* wild type (A), or *plxnd1*^{nz75} (B) larvae. (A′-B′) Inset of red dashed box in A-B, showing LECs within the OLV (*lyve1b*- magenta, *fli1a:nlsEGFP* – green). Yellow arrowheads indicate OLV nuclei. **(C)** Quantitation of facial LEC number at 6 dpf. **(D)** Quantitation facial LEC number from 3- 6 dpf. **(E)** Quantitation of trunk LEC number at 6 dpf. n.s $p > 0.05$, * $p< 0.05$, ** $p< 0.01$ by One-way ANOVA test; error bars indicate s.d. Scale bar = 50 μm. LEC = lymphatic endothelial cell, OLV = otolithic lymphatic vessel. Numbers in graphs represent numbers of larvae.

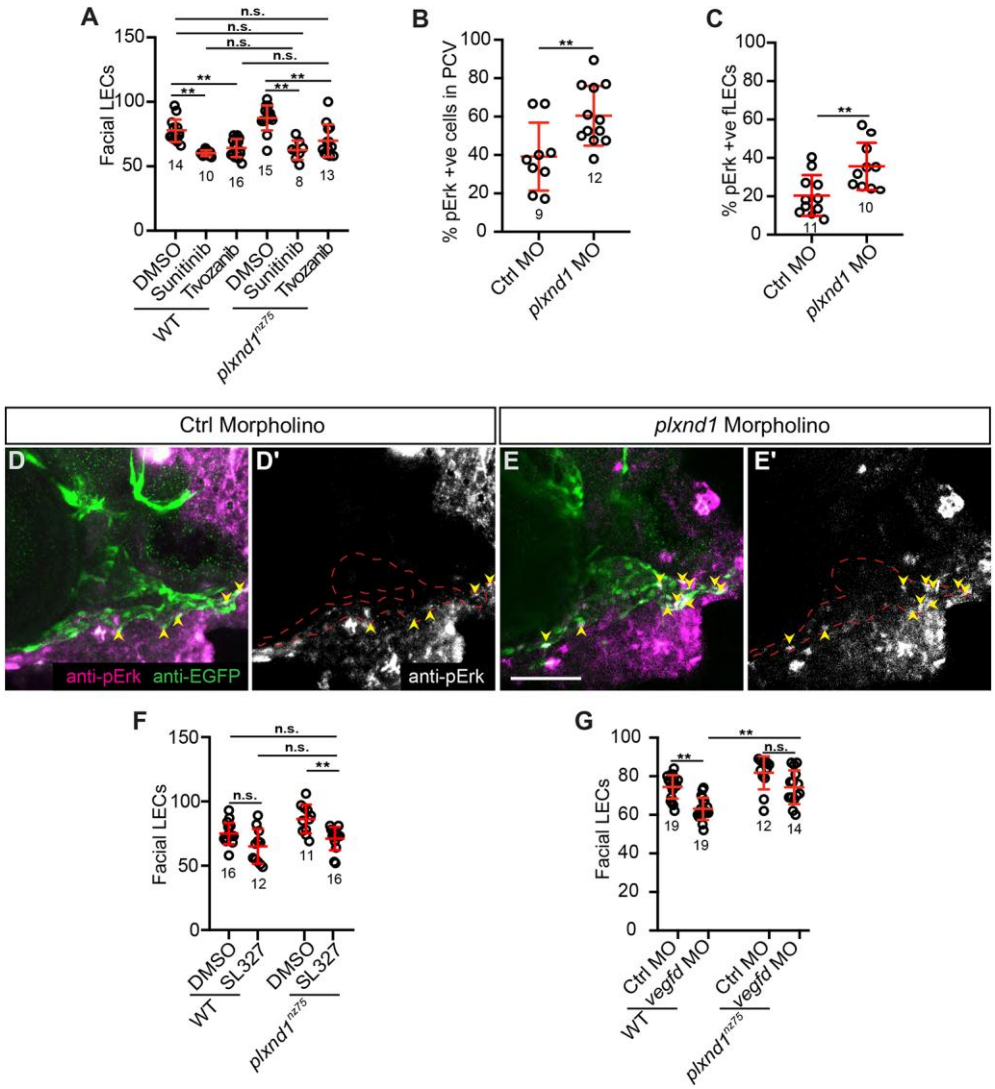

Fig. 5. *plxnd1* mutants have elevated Vegfr/Erk signalling in the facial lymphatics

(A) Quantitation of facial LEC number in 6 dpf larvae treated from 3- 6 dpf with either DMSO, 1 µM sunitinib or 2 nM tivozanib. (**B-C**) Quantitation of the proportion of pErk positive cells within the PCV at 36 hpf (B) or the facial LECs at 3 dpf (C). **(D-E)** Confocal images of anti-pErk (magenta) and anti-EGFP (green) staining in the head at 3 dpf of either control (D) or *plxnd1* (E) *lyve1b:EGFP* morphant larvae. (D′-E′) show anti-pErk staining only. Yellow arrowheads highlight the pErk cells within the facial lymphatics. **(F)** Quantitation of facial LEC number in 6 dpf larvae treated

from 3- 6 dpf with either DMSO or 5 μM SL327. **(G)** Quantitation of facial LEC number in *lyve1b:DsRed; fli1a:nlsEGFP* larvae injected with either control or *vegfd* morpholinos. n.s $p > 0.05$, * $p < 0.05$, ** $p < 0.01$, *** $p < 0.001$ by t-tests, Kruskal-Wallis and ANOVA tests; error bars indicate s.d. Scale bar = 50 μm. LEC = lymphatic endothelial cell. Numbers in graphs represent numbers of larvae.

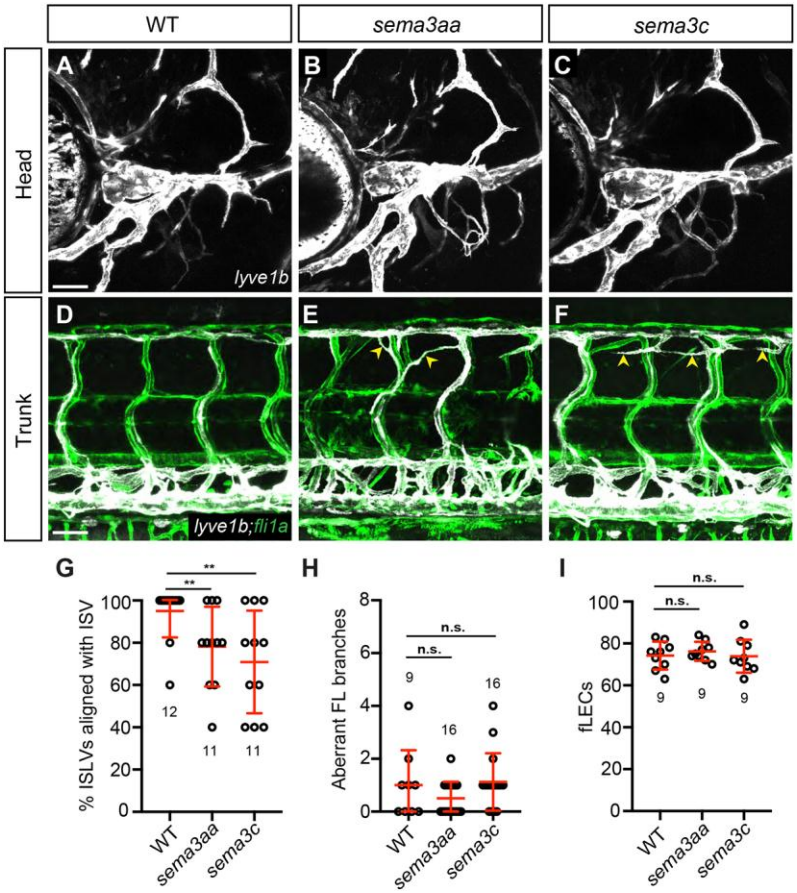

Fig. 6. Semaphorin3 ligands regulate lymphatic growth and guidance

(A-H) Confocal images of the head (A-C) or trunk (D-F) vasculature showing the blood (green) and *lyve1b*-expressing vessels (white) in 6 dpf *lyve1b:DsRed; fli1a:EGFP* wild type (A, D), *sema3aa*^{sa10241} (B, E), or *sema3c*^{sa15161} mutants (C, F). Yellow arrowheads indicate misaligned ISLVs. **(G)** Quantitation of misaligned ISLVs at 6 dpf. **(H)** Quantitation of aberrant facial lymphatics at 6 dpf. **(I)** Quantitation of facial LEC number at 6 dpf. n.s $p>0.05$, * $p< 0.01$, by Mann-Whitney test; error bars indicate s.d. Scale bar = 50 μm. ISLV = intersegmental lymphatic vessel. Numbers in graphs represent numbers of larvae.

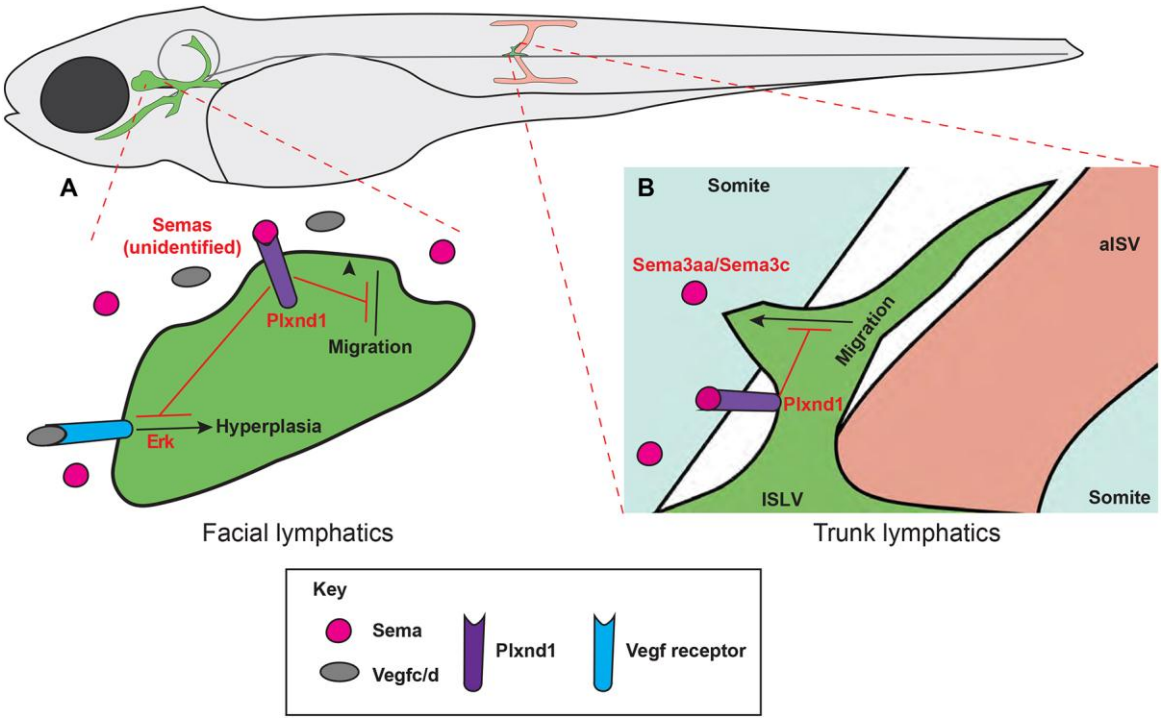

Fig. 7. Plxnd1 signalling regulates lymphatic vessel guidance and growth.

Model of Plxnd1-mediatated regulation of lymphatic development. (**A**) In the head, Plxnd1 signalling antagonises Vegfr/Erk signalling to prevent facial lymphatic hyperplasia. It also prevents aberrant cell migration. The role and identity of Sema ligands in facial lymphatic development are yet to be determined. (**B**) In the trunk, Plxnd1 signalling within developing ISLVs, likely triggered by Sema3aa/Sema3c ligands, prevents migration into the somites.

Sup Fig. 1

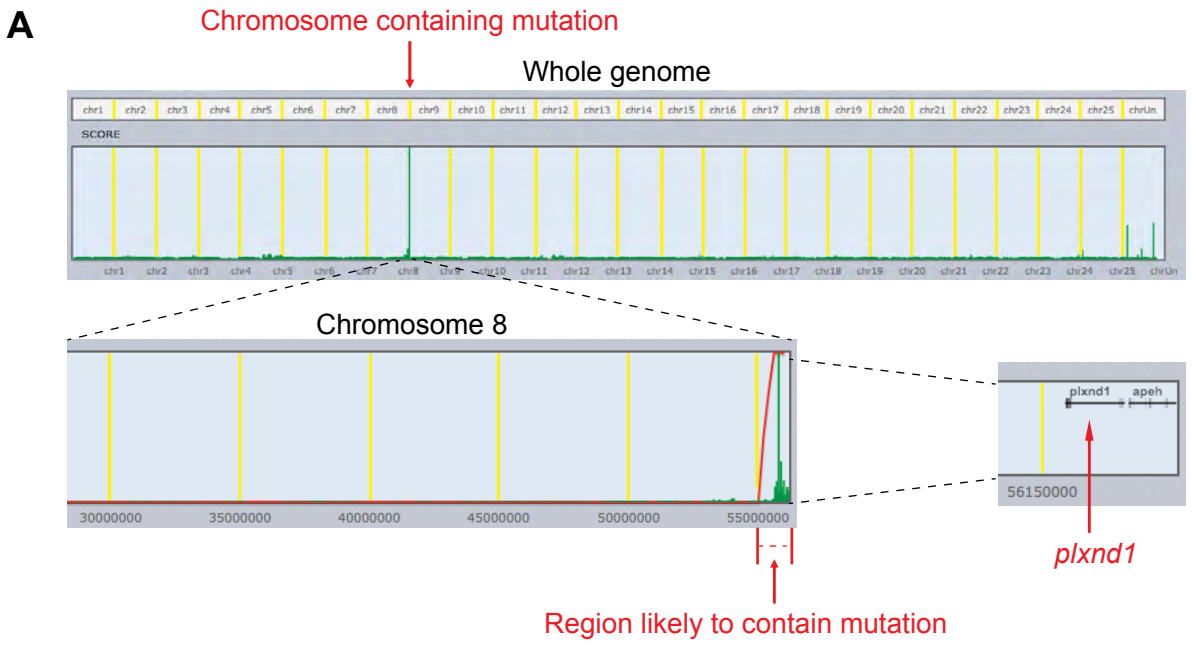

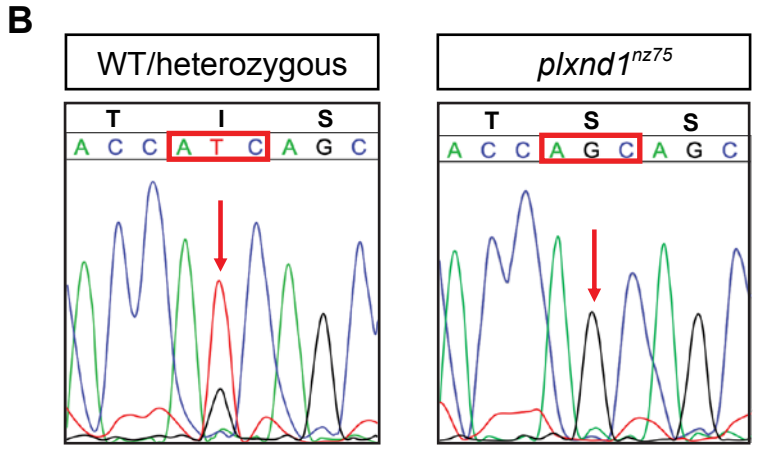

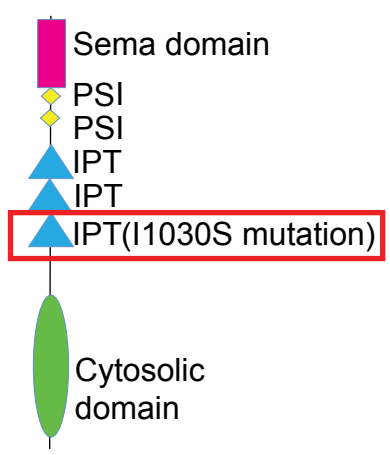

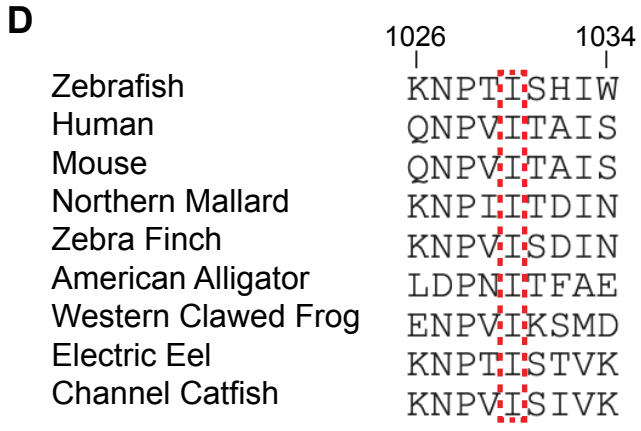

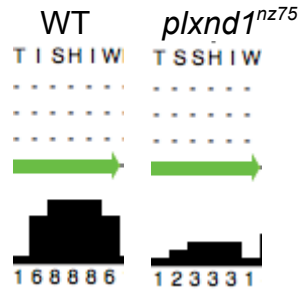

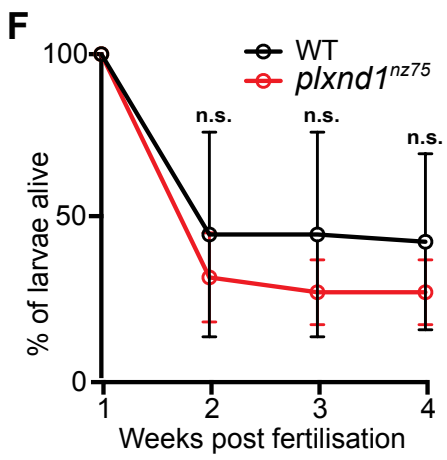

Fig. S1. The *nz75* lymphatic guidance mutant maps to *plxnd1*

(A) Screenshots of the SNPtracker analysis of *nz75* linkage analysis using wild type vs. mutant genomic sequence. The top panel shows homozygosity scores (green) across the whole genome with a clear spike at the end of chromosome 8 (red arrow). The bottom panels show the telomeric region of chromosome 8 that has a high probability of containing the causal mutation (outlined by the red line). This region contains *plxnd1*. **(B)** Sequence chromatograms showing

the *plxnd1* sequence from either wild type/heterozygous or *plxnd1*^{nz75} animals. **(C)** Schematic of Plxnd1 protein domains, with the location of the amino acid change in *plxnd1*^{nz75} annotated.(**D**) Protein sequence alignment by ClustalW highlighting the conserved isoleucine residue mutated in the *plxnd1*^{nz75}mutant (I1030S). **(E)** Secondary structure prediction of the amino acid sequence of Plxnd1 in wild type and *plxnd1*^{nz75} mutants by Jpred4, numbers below the figure indicate higher probability of forming Beta-sheet in the wild type sequence compared to

mutants. (**F**) Kaplan-Meier curves showing the number of larvae alive up to 4 weeks post-fertilisation (n > 20). (**G-H**) Photos showing 6 month old wild type (F) and *plxnd1*^{nz75} (G) fish. n.s = p > 0.05, by a Mann-Whitney test; error bars indicate s.d. Scale bars: 5 mm.

Sup Fig. 2

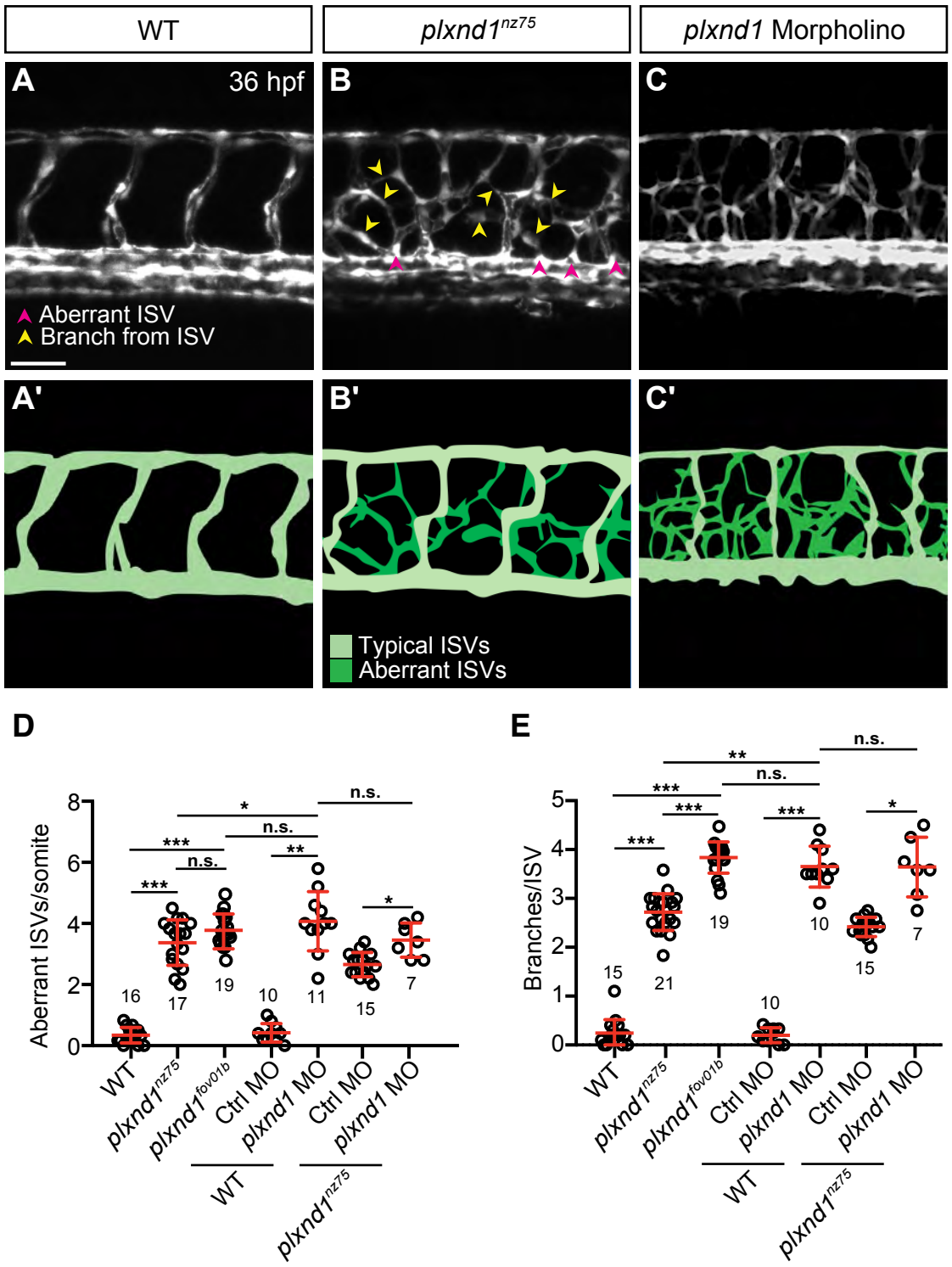

Fig. S2. *plxnd1* mutants and morphants have an increase in ISV number and branching

(A-C) Confocal images of the trunk vasculature in 36 hpf *kdrl:EGFP*- wild type (A), *plxnd1*^{nz75} (B) or *plxnd1* morphant (C) larvae. Arrowheads indicate aberrant ISVs (magenta) and ISV branches (yellow). (A′-C′) Schematics highlighting the vessels in each corresponding confocal image. **(D-E)** Quantitation of aberrant ISVs (D) and ISV branches at 48 hpf. n.s $p > 0.05$, * $p < 0.05$, ** $p < 0.01$, *** $p < 0.001$ by Mann-Whitney test; error bars indicate s.d. Scale bar = 50 µm. ISV = intersegmental vessel. Numbers in graphs represent numbers of larvae.

Sup Fig. 3

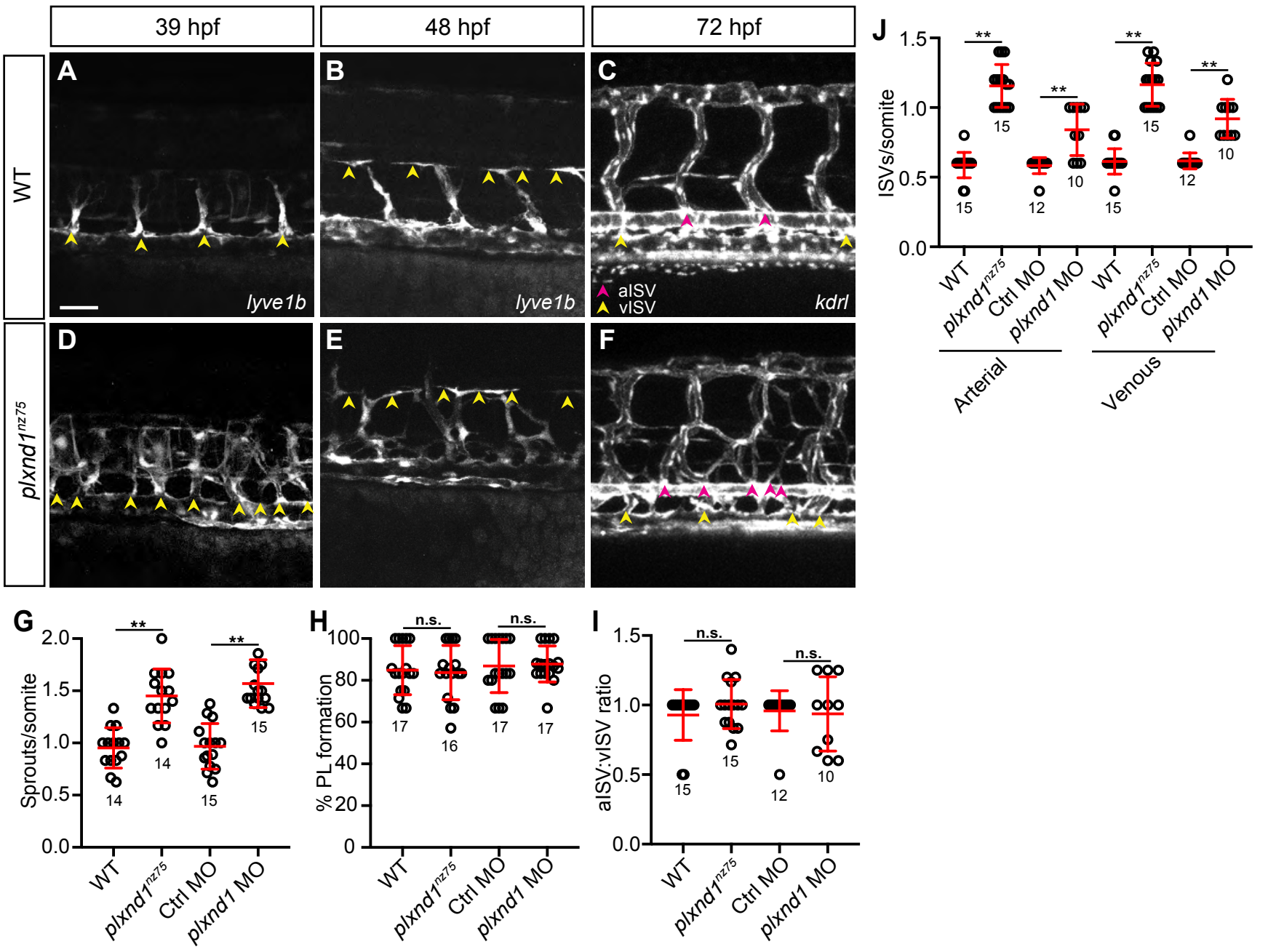

Fig. S3. *plxnd1* mutants and morphants have increased secondary sprouting

(A-F) Confocal images of the trunk vasculature in wild type (A-C) or *plxnd1*^{nz75} (D-F) larvae showing *lyve1b:EGFP* expression at 39 hpf (A, D) or 48 hpf (B, E) or *kdrl:EGFP* expression at 72 hpf (C, F). Yellow arrowheads highlight either the secondary sprouts (A, D), parachordal LECs (B, E) or venous ISVs (C, F) while magenta arrowheads highlight the arterial vessels (C, F). **(G)** Quantitation of secondary sprouts at 39 hpf. **(H)** Quantitation of parachordal LECs at 48 hpf. **(I)** Quantitation of the ratio of arterial ISVs to venous ISVs (vISVs) at 72 hpf. **(J)** Quantitation of the number of arterial ISVs and venous ISVs per somite at 72 hpf. n.s $p > 0.05$, ** $p < 0.01$ by Mann-Whitney test; error bars indicate s.d. Scale bar = 50 μm. ISV = intersegmental vessel, PL = parachordal LEC. Numbers in graphs represent numbers of larvae.

Sup Fig. 4

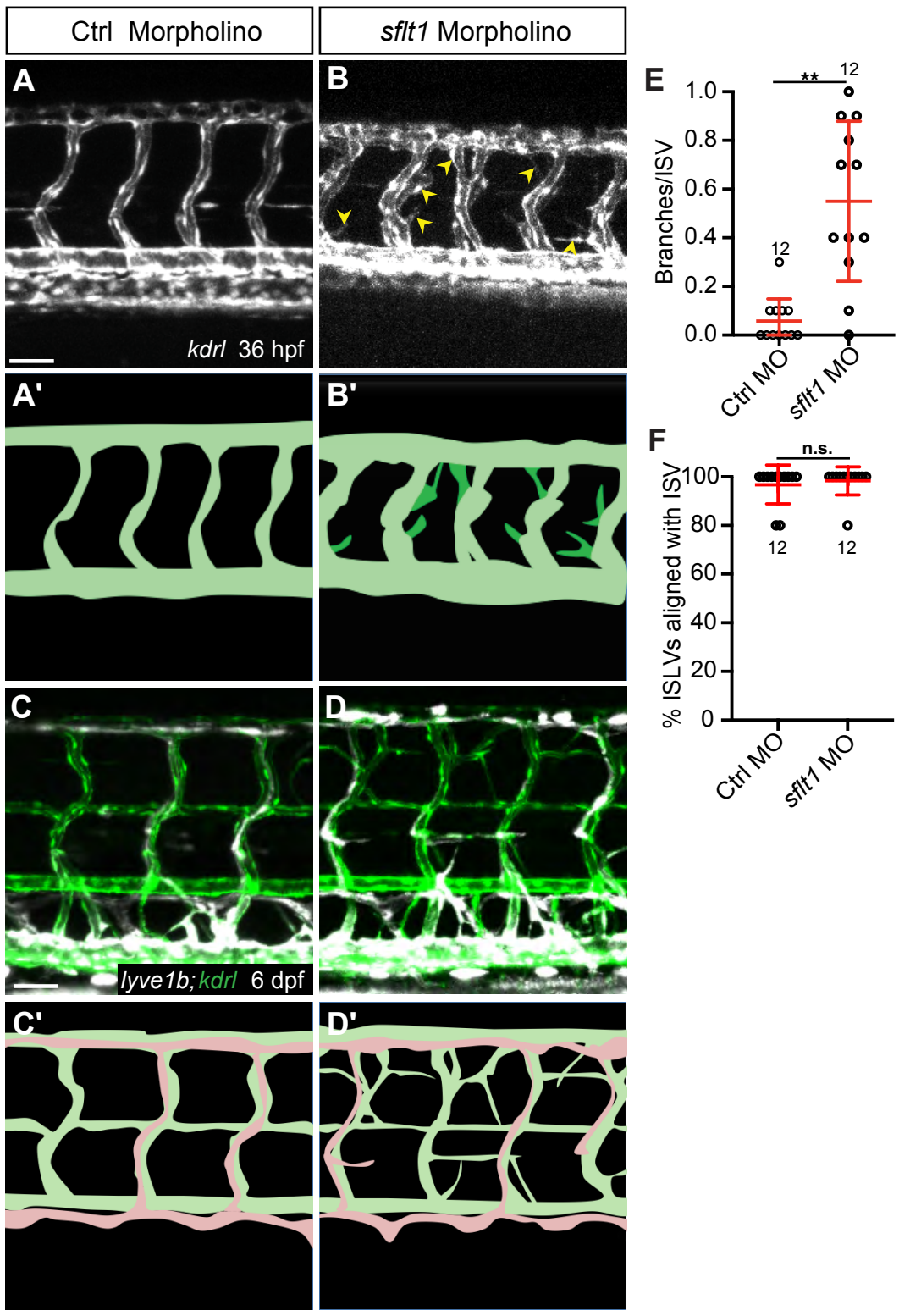

Fig. S4. The ISLVs in *sflt1* morphants align with blood vessels

(A-B) Confocal images of the trunk vasculature in 36 hpf *kdrl:EGFP*- control (A) or *sflt1* morphants (B). (A′-B′) Schematics highlighting the aberrant ISVs in each corresponding confocal image. **(C-D)** Confocal images of the blood (*kdrl*-green) and *lyve1b*-expressing vessels (white) in the trunks of 6 dpf *lyve1b:DsRed; kdrl:EGFP* control (C) or *sflt1* morphants (D). (C′-D′) Schematics highlighting the aberrant and misaligned vessels in each corresponding confocal image. **(E)** Quantitation of ISV branches at 48 hpf. **(F)** Quantitation of misaligned ISLVs at 6 dpf (n=12). n.s $p>0.05$, ** $p< 0.01$ by t- test; error bars indicate s.d. Scale bar = 50 μm. ISV = intersegmental vessel, ISLV = intersegmental lymphatic vessel. Numbers in graphs represent numbers of larvae.

Sup Fig. 5

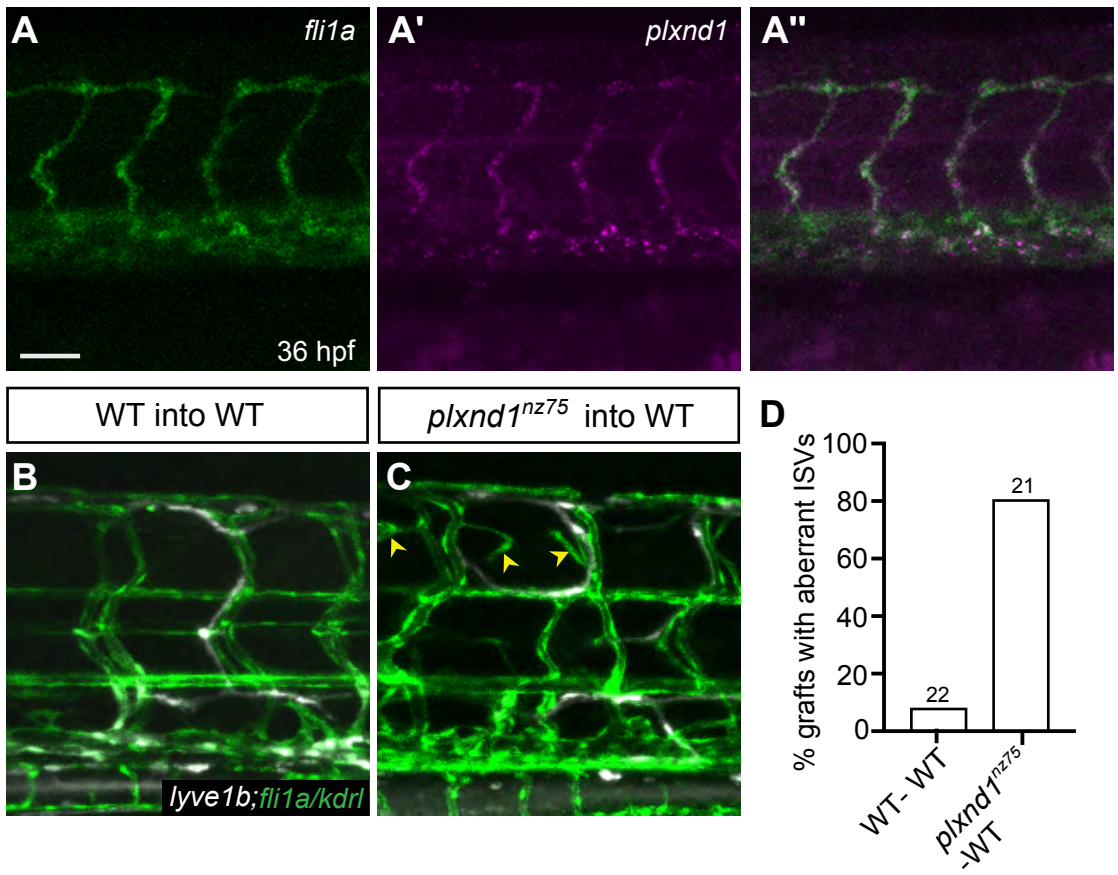

Fig. S5. *plxnd1* is expressed in ISVs

(**A**) Confocal images of the *fli1a:EGFP* expression (anti-*EGFP* - green) (A), *plxnd1* expression (anti-*plxnd1* – magenta) (A′) or both (A′′) in the trunk of 36 hpf *fli1a:EGFP* larvae. **(B-C)** Confocal images of the trunk vasculature in chimeric animals at 6 dpf showing donor-derived LECs (*lyve1:DsRed* - white) and either donor derived or host derived BECs (green) from either wild type (B) or *plxnd1*^{nz75} (C) donors. Note the aberrant ISVs in the *plxnd1*^{nz75} -derived grafts, highlighted by the yellow arrowheads in C. **(D)** Quantitation of the percentage of grafted animals (containing *lyve1:DsRed* cells) that displayed aberrant ISVs. Numbers in graphs represent numbers of larvae.

Sup Fig. 6

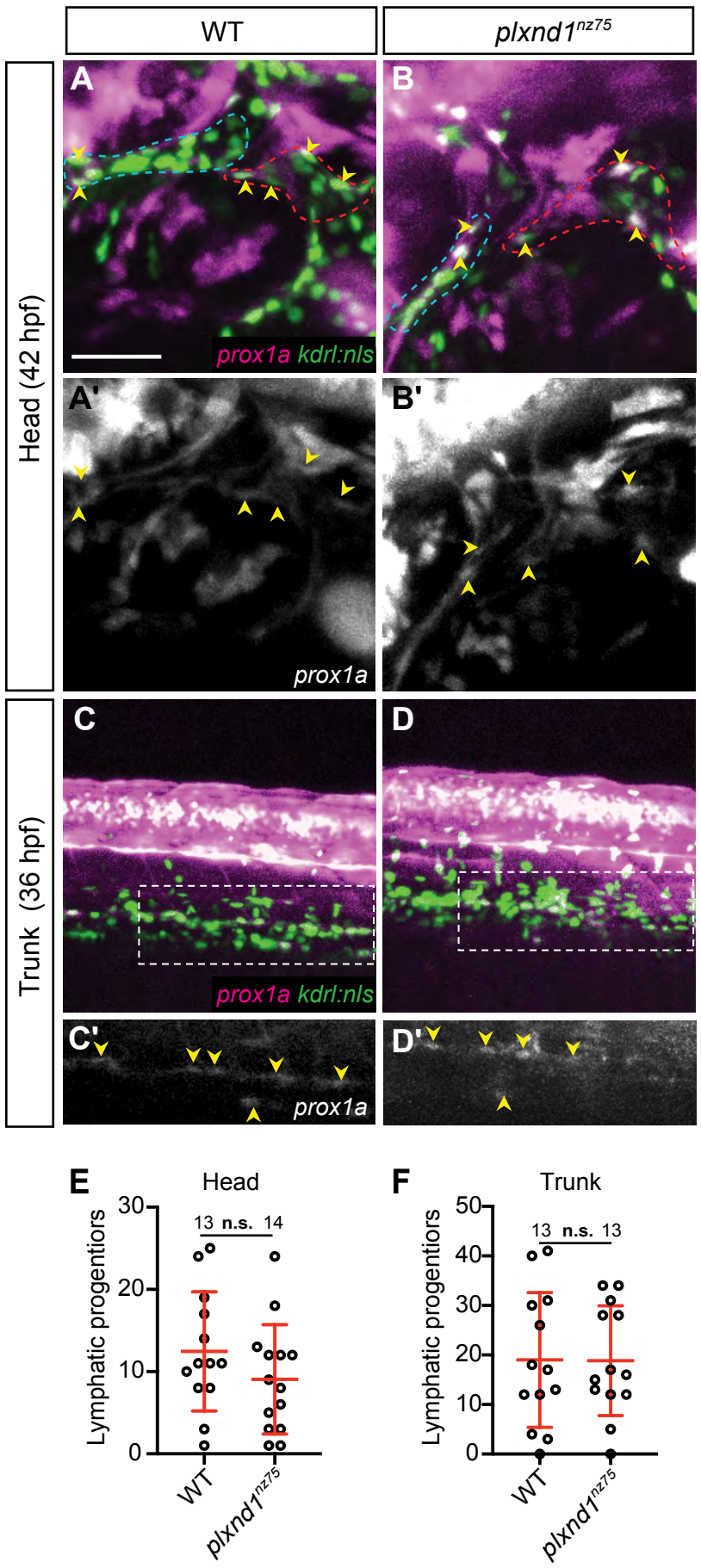

Fig. S6. *plxnd1* mutants have normal levels of lymphatic specification

(A-D) Confocal images of the endothelial nuclei (green) and *prox1a* expression (magenta) in the head at 42 hpf (A-B) or the trunk at 36 hpf (C-D) of either wild type (A,C) or *plxnd1*^{nz75} (B,D) *prox1a:Venus; kdrl:nlsmCherry* larvae. The primary head sinus (blue dashed line) and facial lymphatic sprout (red dashed line) are highlighted in A-B, while a white dashed outline in C-D indicates a section of the PCV that will be highlighted in C-D. (A-D) *prox1a* expression only (grey), yellow arrowheads indicate lymphatic progenitors co-expressing *prox1a:Venus* and *kdrl:nlsmCherry*. (E) Quantitation of lymphatic progenitors in the head at 42 hpf. (F) Quantitation of lymphatic progenitors in the trunk (PCV) at 36 hpf. n.s $p>0.05$, by t-test; error bars indicate s.d. Scale bar = 50 μm. PCV = posterior cardinal vein. Numbers in graphs represent numbers of larvae.

Sup Fig. 7

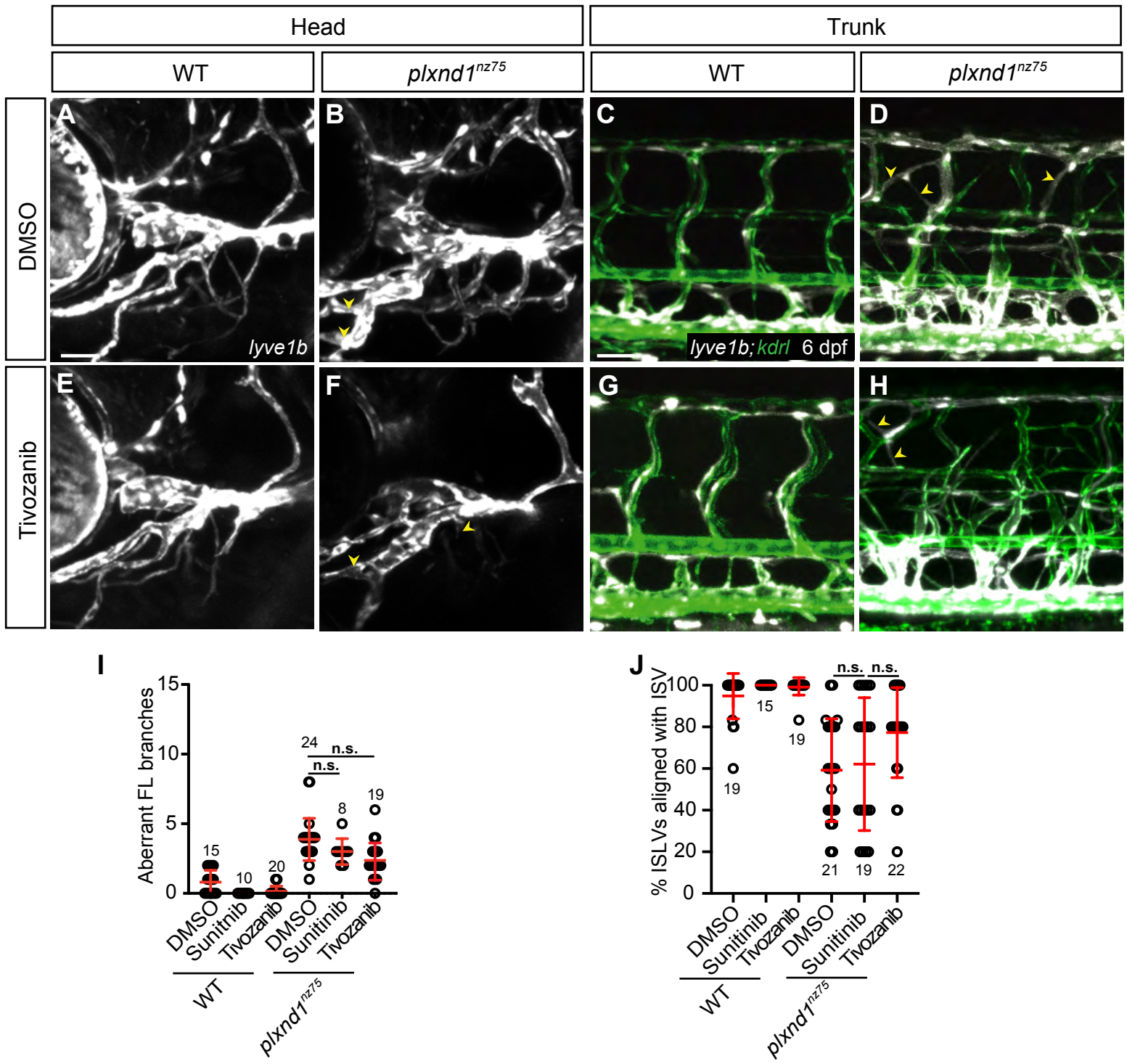

Fig. S7. Vegfr inhibition does not reduce the frequency of lymphatic misguidance. (A-H) Confocal images of the head (A-B, E-F) and trunk (C-D, G-H) vasculature in 6 dpf wild type (A, C, E, G) or *plxnd1*^{nz75} (B, D, F, H) *lyve1b:DsRed* (white)*; kdrl:EGFP* (green) larvae treated with either DMSO (A-D) or 2 nM tivozanib (E-H). Yellow arrowheads highlight aberrant facial lymphatics (B,F) or misaligned ISLVs (D, H). **(I-J)** Quantitation of the number of aberrant facial lymphatic branches (I) and of misaligned ISLVs (J) ($n \geq 11$). n.s $p > 0.05$ by Kruskal-Wallis test; error bars indicate s.d. Scale bars: 50 µm. ISLV = intersegmental lymphatic vessel. Numbers in graphs represent numbers of larvae.

Sup Fig. 8

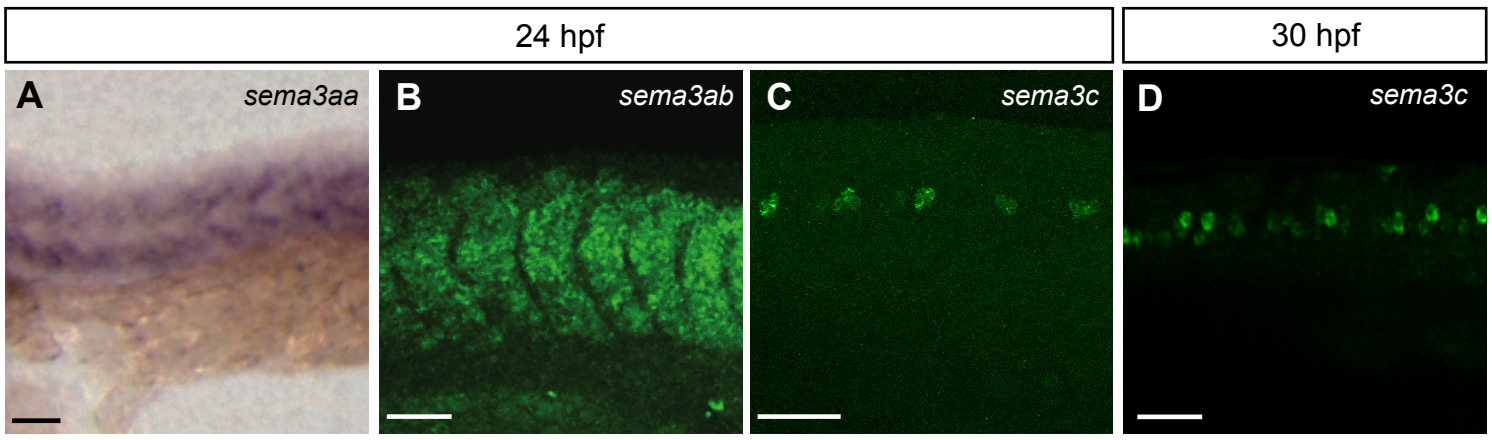

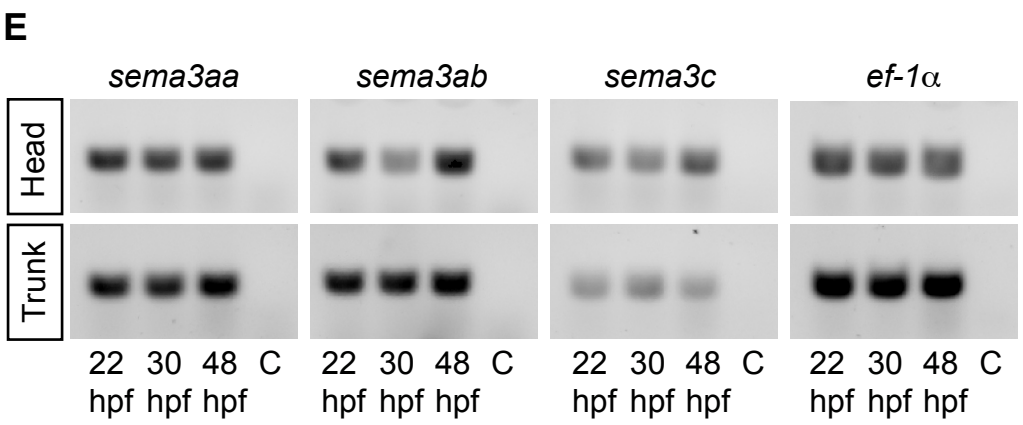

Fig. S8. *sema3aa*, *sema3ab* and *sema3c* are expressed in the zebrafish trunk.

(**A**) Brightfield or (**B-D**) confocal images of *sema3aa*, *sema3ab* or *sema3c* expression in trunks of either 24 hpf (A-C) or 30 hpf (D) larvae. (**E**) Gel pictures (inverted colour) of RT-PCR products from RNA isolated from either dissected heads or trunks of zebrafish larvae at either 22, 30 or 48 hpf. All PCR products match the predicted cDNA size (*sema3aa* = 93bp, *sema3ab* = 111bp, *sema3c* = 82bp). C = no template control. Scale bars: 50 μm.

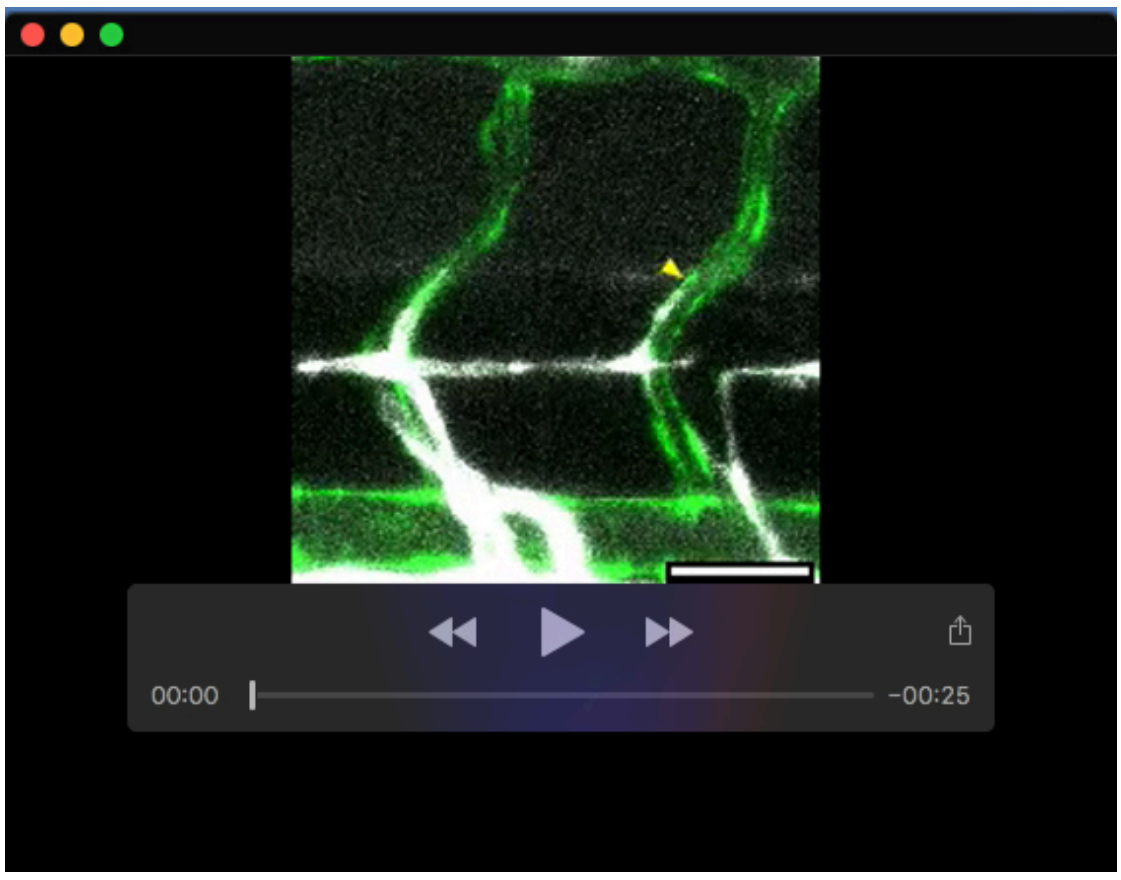

Movie 1. ISLV growth in a wild type embryo.

Confocal time-lapse imaging from 60 to 70 hpf of the trunk of a *lyve1b:DsRed; kdrl:EGFP* embryo displaying lymphatics (white) and blood vessels (green). Yellow arrowhead indicates the ISLV tip. Time-lapse image z-stacks were collected 15 minutes apart; movie was made at 6 frames per second. Stills from movie displayed in Fig. 2. Scale bar = 50 μm.

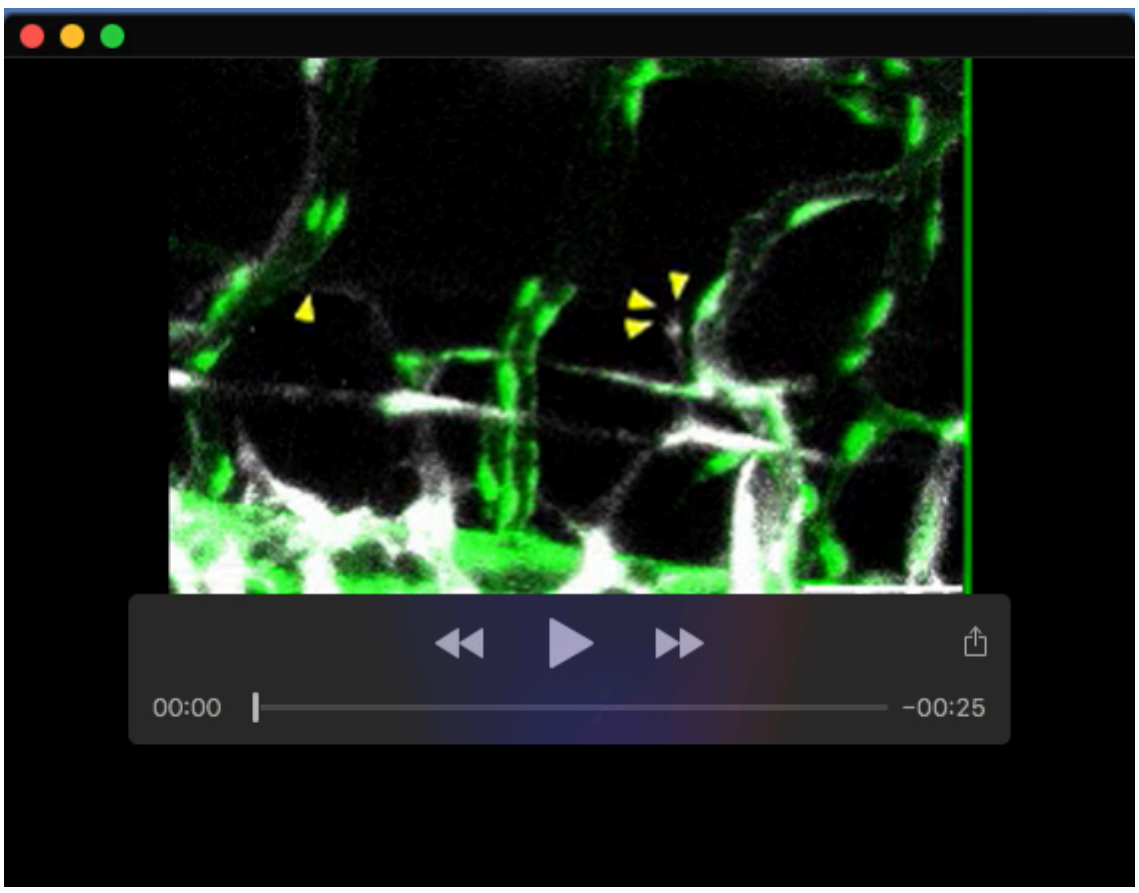

Movie 2. ISLV growth in a *plxnd1* embryo.

Confocal time-lapse imaging from 60 to 74.5 hpf of the trunk of a *plxnd1*^{nz75}; *lyve1b:DsRed; kdrl:EGFP* embryo displaying lymphatics (white) and blood vessels (green). Yellow arrowheads indicates the ISLV tips. Time-lapse image z-stacks were collected 15 minutes apart; movie was made at 6 frames per second. Stills from movie displayed in Fig. 2. Scale bar = 50 μm.

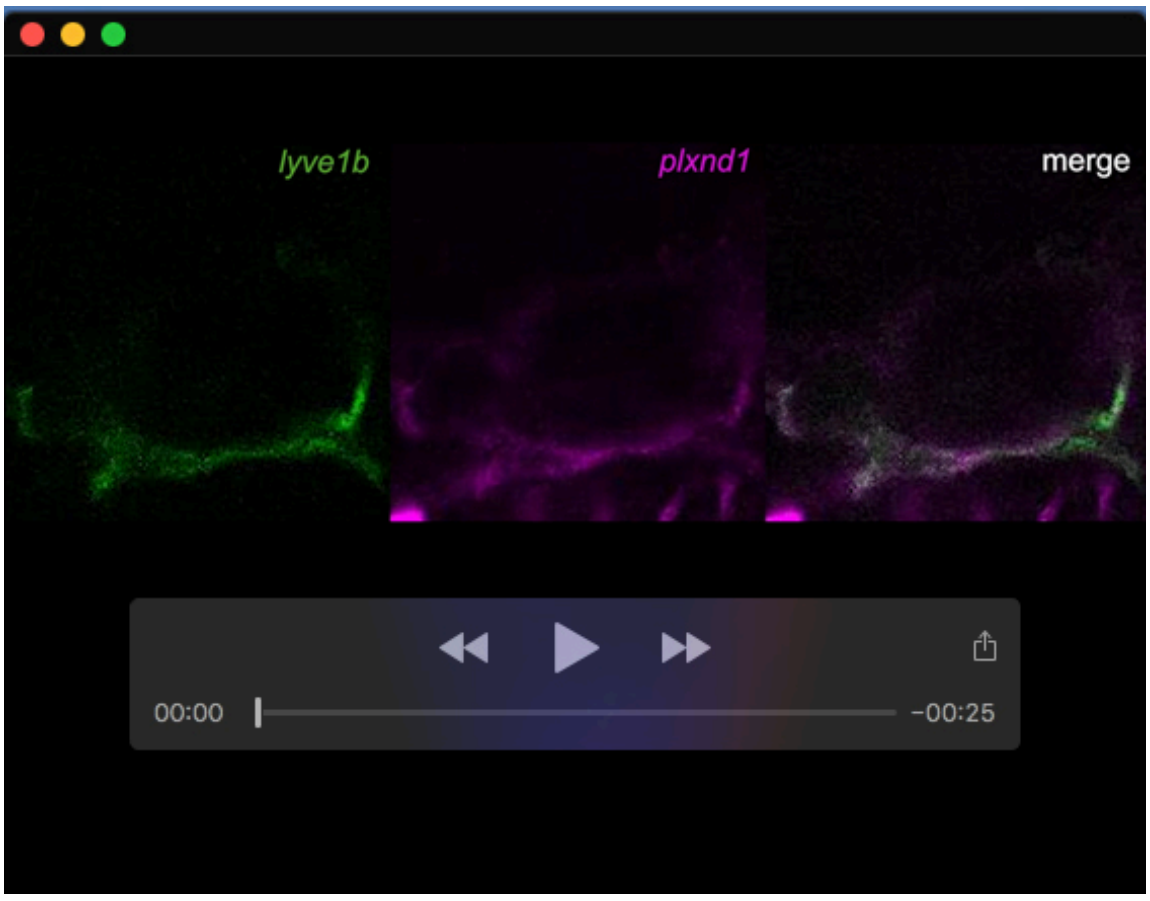

Movie 3. *plxnd1* expression in the head

Movie of the confocal z-stack from Figure 3A showing *lyve1b:EGFP* expression (anti-*EGFP* - green), *plxnd1* expression (anti-*plxnd1* – magenta) or both in the head of a 48 hpf *lyve1b:EGFP* embryo.

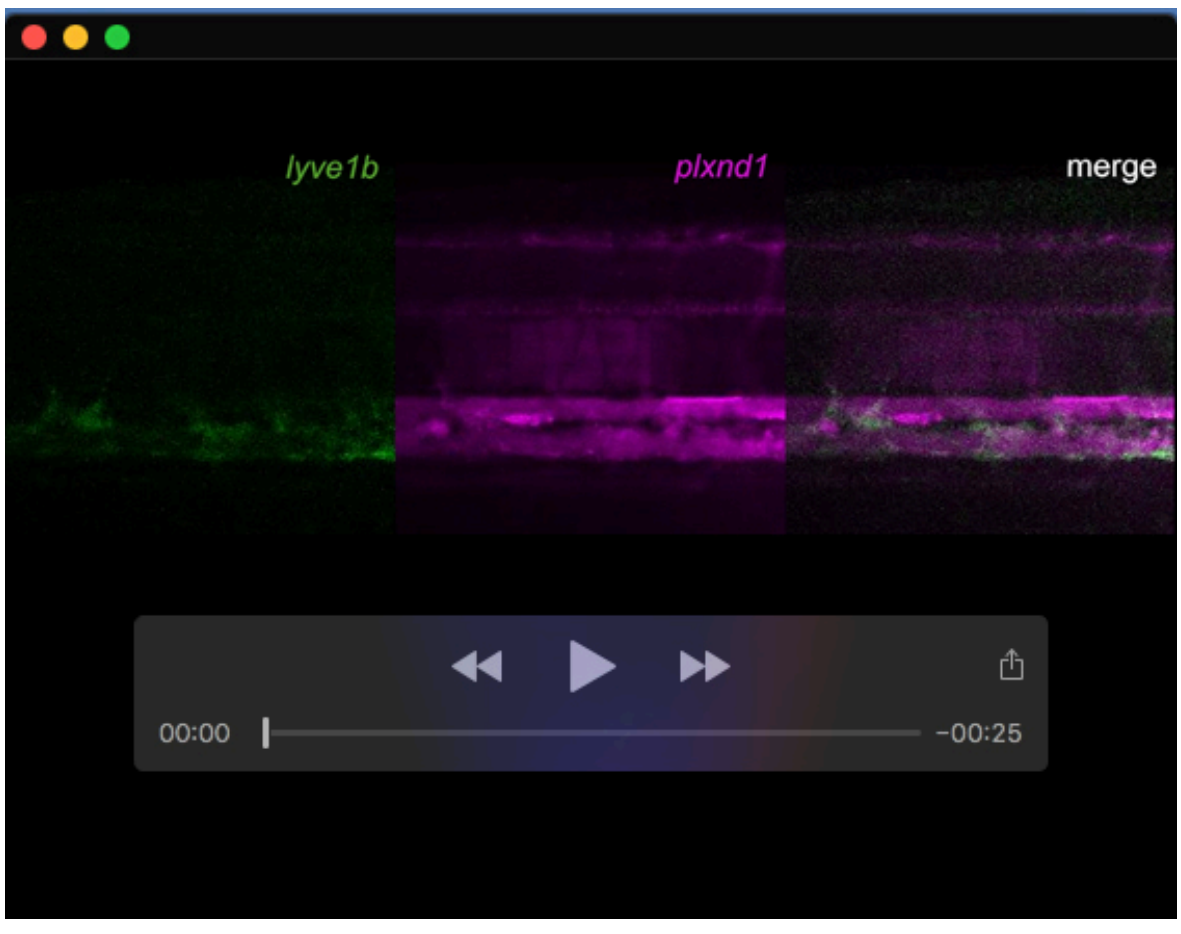

Movie 4. *plxnd1* expression in the trunk

Movie of the confocal z-stack from Figure 3B showing *lyve1b:EGFP* expression (anti-*EGFP* - green), *plxnd1* expression (anti-*plxnd1* – magenta) or both in the trunk of a 48 hpf *lyve1b:EGFP* embryo.